Chapter 5

Smart Foam as an Active/Passive Liner for Duct Acoustic Control: *Numerical & Experimental Studies*

5.1 Introduction

An advanced noise control application is addressed in this chapter which employs smart foam to suppress the sound propagation in a rectangular, anechoically-terminated duct. The importance of this experimental study is that it will provide a basis for the implementation of smart foam in noise control applications involving irregularly shaped cavities such as is found in the interior of an aircraft cabin or jet engine inlets. In the following experiments, a collective array of smart foam modules located on an interior wall of the duct are used to attenuate the transverse propagating acoustic modes within the enclosure. The excitation is provided by an acoustic driver located in the duct wall opposing the anechoic termination. An investigation of harmonic and broadband noise control is performed by minimizing the sound pressure at a number of transverse points downstream of the smart foam array. A digital control approach is implemented and is governed by the Filtered x LMS algorithm. A discussion of the results, followed by a comparison with similar numerical simulations is provided.

5.2 Duct Properties and Construction

The rigid duct used in this study may be classified as a long, rectangular waveguide as shown in Figure 5.1. It is manufactured from 0.75 in. (thickness) high-density, particle board sheets. The interior dimensions of the duct are 6.0 in. (width) x 41.375 in. (height) x 12.0 ft (length). A 6.0 in. (diameter) acoustic driver is mounted in the upper, left corner of the duct and represents the primary noise source. Four sets of 2.0 in. (thickness) x 4.0 in. (width) x 41.375 in. (height) longitudinal, wooden stiffeners are attached to the exterior of the duct to offer extra support for the side walls in order to approximate rigid wall boundary conditions (see Figure 5.2(a)).

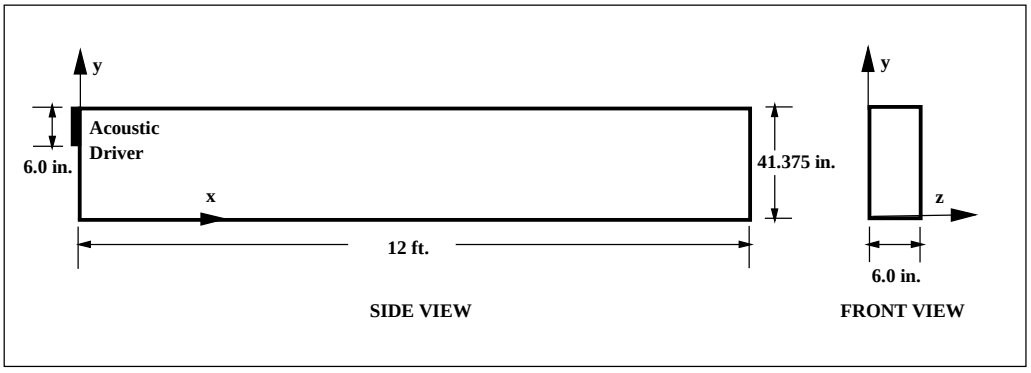

Figure 5.1 Interior dimensions of duct.

In the following experiments, a particular section of the duct bottom wall is lined with a collective array of smart foam modules while the remainder of the bottom wall is treated with homogeneous, sound absorbing foam. Note that the components of the active/passive liner (i.e. partially-reticulated foam and PVDF) are identical to the components of smart foam used in the previous experiments. It is desired that the interior dimensions of the unlined, rigid duct be equal to the interior dimensions of the duct with the active/passive liner. To accomplish this, a removable rigid, wooden insert is manufactured to rest on the floor of the duct. This removable insert measures 6.0 in. (width) x 2.0 inches (height) x 12.0 ft (length) which are the same dimensions as the liner. Consequently, the effective interior dimensions of the duct (*for lined and unlined cases*) are 6.0 in. (width) x 39.375 in. (height) x 12.0 ft (length).The wooden sheets that make up the side walls and floor of the duct are permanently attached using galvanized

nails. The top and end boards are assembled with removable screws to allow access to the duct interior. The acoustic speaker is mounted in the upper, left corner of the duct and represents the primary noise source (see Figure 5.1 and Figure 5.2(b)). This speaker location is chosen so that the transverse acoustic modes of the duct, tabulated in the following section, will be excited and forced to propagate along the duct length. The right end of the duct is outfitted with a triangular, anechoic wedge, as shown in Figure 5.2(c), made of Fiberglas enveloped in a thin, wire mesh frame. The dimensions of the triangular wedge are 6.0 in. (width) x 39.375 (height) x 2.0 ft (length).

(a) (b) (c)

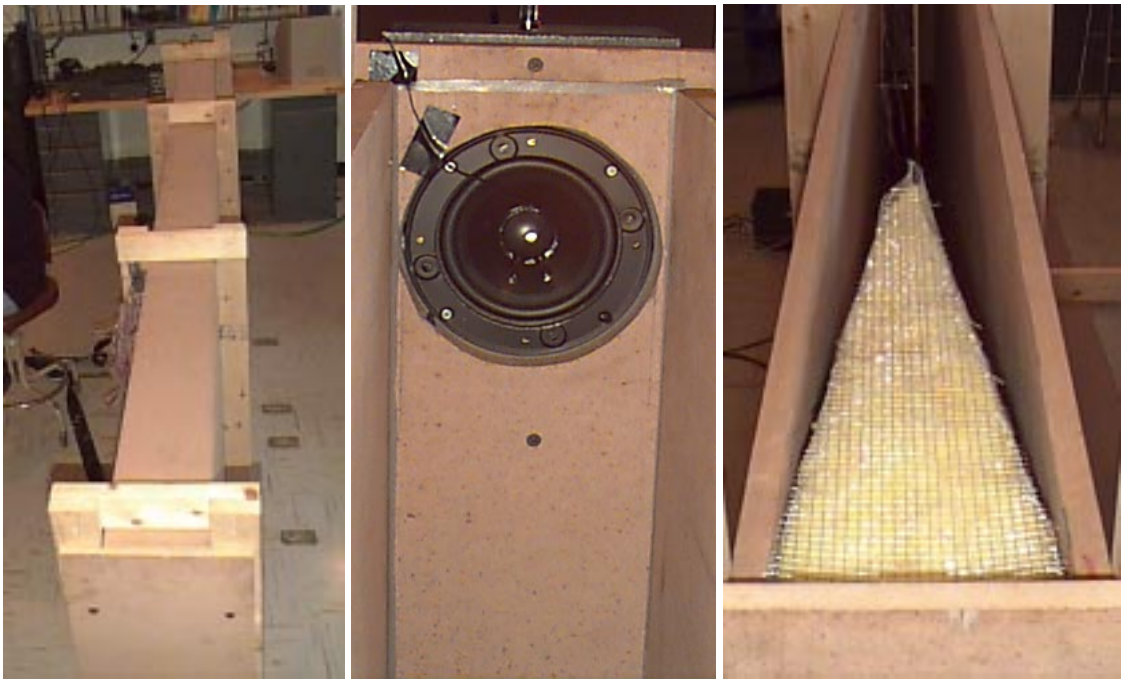

Figure 5.2 (a) Duct in the laboratory. (b) Acoustic speaker in duct end wall. (c) Anechoic wedge at duct termination

5.3 Modal Analysis of Interior Acoustic Field of Duct & Reflection Coefficient Describing Duct Termination

Preliminary experimental testing involved identifying the transverse and longitudinal acoustic modes and corresponding resonance frequencies of the duct in the 50<f<550 Hz frequency range. Examples of the first three one dimensional mode shapes that develop between two opposing duct walls in response to an acoustic disturbance is illustrated in Figure 5.3. These are ideal mode shapes formed by a single plane propagating wave or the interference of multiple, out of phase plane waves which generate higher order modes. Under ideal conditions, there are no reflections from the duct termination which would cause standing waves (i.e. longitudinal mode shapes caused by axially traveling waves impinging on the termination). Therefore, it is also necessary to investigate the efficiency of the anechoic wedge at damping the acoustic reflections at the duct termination in the following modal analysis.

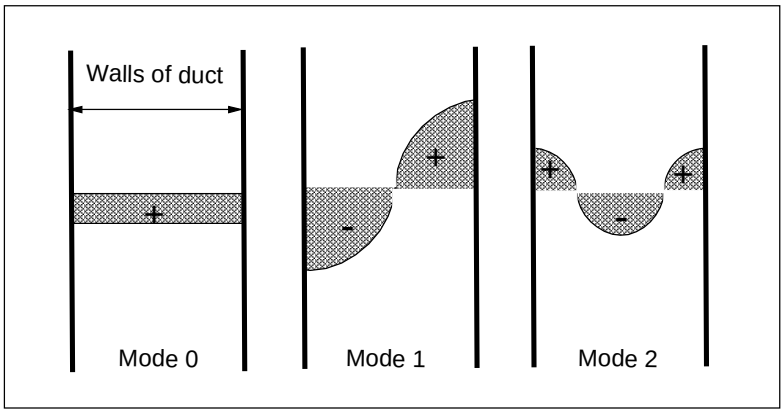

Figure 5.3 Illustration of one dimensional acoustic mode shapes within duct.

The modal analysis required driving the acoustic speaker with broadband random noise and obtaining the sound pressure within the duct over a two-dimensional grid of measurement points (see Figure 5.4). A vertical column of 16 evenly spaced microphones traverses the length of the duct at 2.0 inch intervals to acquire a two-dimensional grid of sound pressure data. In an enclosure, the potential and kinetic energy become infinite, with zero damping, at the resonance frequencies of the system and both energy expressions are approximately equal above the first resonance frequency. Accordingly, only the potential energy is studied to determine the acoustic modes of the duct using the

magnitude, $|p(x,y)|$, of the acoustic pressure at each measurement point. The potential energy within the duct is determined by the expression [79]

$$E_p = S\int_0^{L_x} \frac{|p(x)|^2}{4\rho_o c_o^2} dx \approx S\sum_{n=1}^{N} \frac{|p(x)|^2}{4\rho_o c_o^2} \tag{5.1}$$

where S is the cross sectional area of the duct, the symbol N denotes the number of measurement points in the x direction, ρ_o and c_o are the density and speed of sound in air under standard atmospheric conditions, respectively. The value $|p(x)|$ denotes the magnitude of the average pressure (sum of the squared pressure divided by sixteen) in the y direction at a particular measurement point, x, along the duct. The experiment is repeated for four unique duct configurations: (a) *Rigid duct floor with anechoic termination*, (b) *Rigid duct floor with rigid termination*, (c) *Foam-lined duct floor with anechoic termination* and (d) *Foam-lined duct floor with rigid termination.*

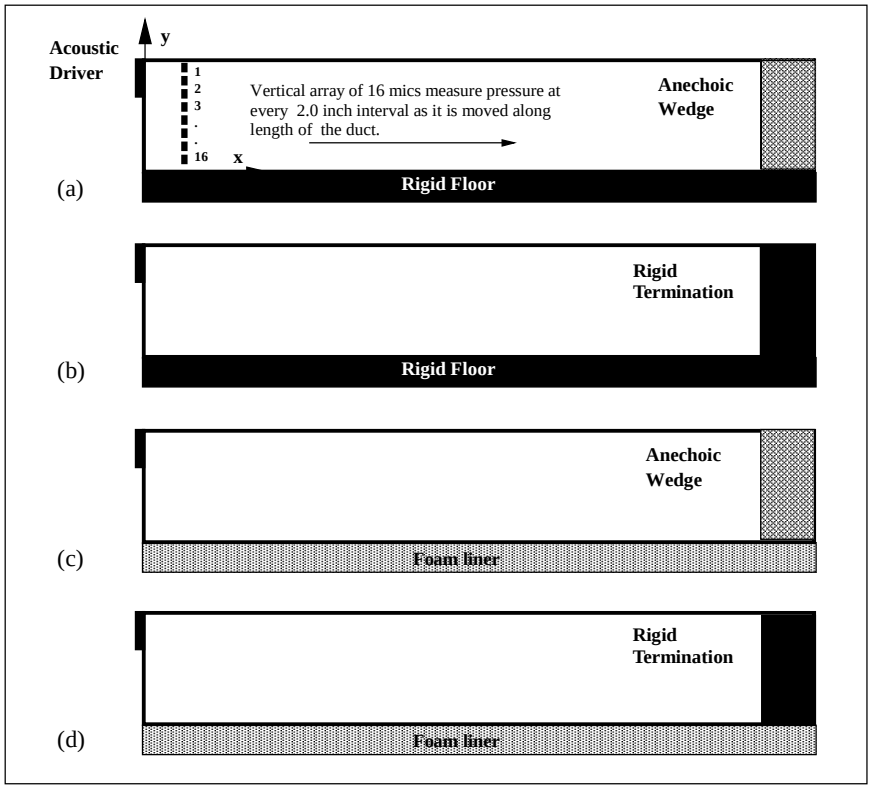

Figure 5.4: The four unique duct configurations used for acoustic modal analysis (a) Rigid duct floor with anechoic termination (b) Rigid duct floor with rigid termination (c) Foam-lined duct floor with anechoic termination (d) Foam-lined duct floor with rigid termination

Plots of the energy versus frequency are studied to identify the transverse and longitudinal acoustic resonance frequencies of the enclosure for the four different duct configurations. Figure 5.5 quantifies the acoustic energy of the system as a function of frequency for the *"Rigid Duct/Rigid End"* and the *"Rigid Duct/Anechoic End"* configurations. When considering the long, rigid duct, it is expected that the transverse acoustic modes of the enclosure remain virtually unchanged by the type of end termination. In other words, the anechoic end should provide considerable damping of only the longitudinal acoustic modes since these are made up of axially traveling waves which directly impinge upon the termination. Accordingly, the transverse acoustic resonant modes and corresponding frequencies are identified by the peaks in each curve where the energy is approximately equal. By process of elimination, the remaining peaks coincide with longitudinal acoustic modes. For these two different duct configurations, the transverse and longitudinal acoustic modes and corresponding resonance frequencies are given in Table 5.1. This data shows that there are three transverse acoustic modes present in the studied frequency range for the rigid duct with an anechoic or rigid termination. It is proven that the anechoic termination has a minimal effect on the transverse acoustic modes in that it lowers the resonance frequencies of the duct by only a few Hertz. In reference to the longitudinal acoustic modes, Table 5.1 indicates that a rigid duct with a rigid end has a high acoustic modal density as there are ten lohgitudinal modes present in the studied frequency range. Comparatively, only the first two longitudinal modes are present for a rigid duct with an anechoic end indicating the efficiency of the anechoic termination at damping the longitudinal modes as the frequency increases. This data further indicates that the anechoic termination considerably lowers the longitudinal resonant frequencies of the system as the frequency increases.

A plot of the acoustic energy versus frequency for the *"Rigid Duct/Anechoic End"* and *"Lined Duct/Anechoic End"* configurations are shown in Figure 5.6. Note that these two duct configurations will be used in the following duct acoustic control experiments. A comparison of these two curves is used to extrapolate the transverse and longitudinal acoustic modes for the foam-lined duct with an anechoic termination. Recall that there are no longitudinal modes above 122 Hz, the second mode for the anechoically-terminated,

rigid duct case. It is further helpful to realize that in the very low-frequency range, the effects of the liner on the longitudinal modes should be minimal (i.e. mode shape and resonance frequency are virtually the same for the lined and unlined, anechoically terminated duct). With this information, Figure 5.6 is utilized to characterize the transverse and longitudinal acoustic modes for the foam-lined duct with an anechoic termination. The results are listed in Table 5.1.

The modes and corresponding resonance frequencies for all the duct configurations have been identified except for the lined duct with a rigid end. The acoustic energy versus frequency for the *"Lined Duct/Rigid End"* and *"Lined Duct/Anechoic End"* is illustrated in Figure 5.7, and is used to identify these unknown modes. Recall that all modes corresponding to the "Lined Duct/Anechoic End" configurations are known. Furthermore, it has been proven that there are no longitudinal modes above the second resonance frequency for the anechoically-terminated duct. One can extract the transverse modes for the lined duct with a rigid end by the peaks in each curve where the energy is approximately equal. Then, by process of elimination the peaks that are effected by the anechoic end represent the longitudinal modes of the lined duct with a rigid end. The transverse and longitudinal modes of the lined duct with rigid end are given in Table 5.1.

All the modes of the four unique duct configurations have been identified. However, in the interest of completeness, Figure 5.8 compares the acoustic energy of the system as a function of frequency for the *"Rigid Duct/Rigid End"* and the *"Lined Duct/Rigid End"* configurations. A comparison of the two curves, indicates that the damping of the acoustic response in the interior of the duct provided by the liner increases significantly as the excitation frequency increases. This supports that fact that the sound attenuation within the long, foam-lined duct is dependent on the wavelength of the propagating sound waves relative to the length of the duct.

The information given in Table 5.1 is important and it will be referred to in the following duct acoustic control experiments to identify the appropriate test frequencies. In particular, the goal of the tests are to show that simultaneous active/passive sound

control, established with smart foam, can successfully attenuate the transverse propagating modes of the lined, anechoically-terminated duct.

Table 5.1 Transverse & longitudinal acoustic duct resonance frequencies corresponding to the first unique duct configurations

TRANSVERSE MODES				
Mode	Rigid Duct & Anechoic End	Rigid Duct & Rigid End	Lined Duct & Anechoic End	Lined Duct & Rigid End
1	188	189	184	184
2	356	358	342	341
3	526	529	504	503
LONGITUDINAL MODES				
Mode	Rigid Duct & Anechoic End	Rigid Duct & Rigid End	Lined Duct & Anechoic End	Lined Duct & Rigid End
1	104	110	102	108
2	122	152	121	148
3	-	240	-	198
4	-	262	-	238
5	-	286	-	254
6	-	332	-	286
7	-	399	-	362
8	-	422	-	404
9	-	499	-	444
10	-	516	-	488

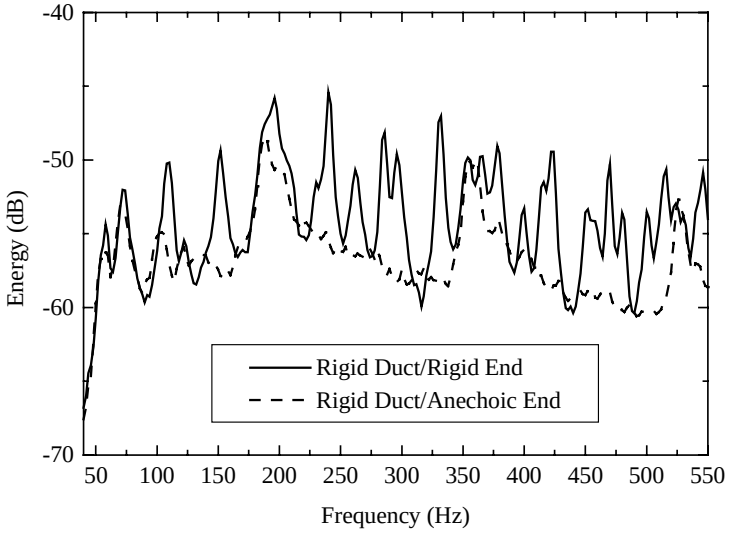

Figure 5.5: Comparison of acoustic energy vs. frequency for Rigid Duct/Rigid End and Rigid Duct/Anechoic End configurations.

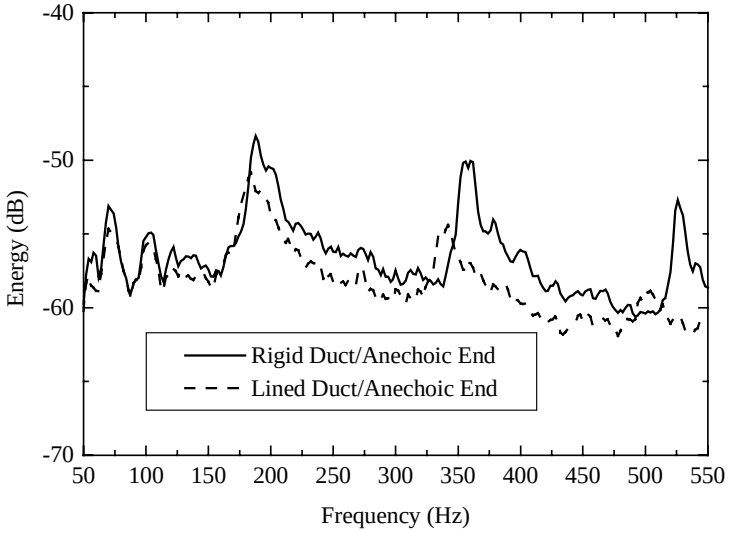

Figure 5.6: Comparison of acoustic energy vs. frequency for Rigid Duct/Anechoic End and Lined Duct/Anechoic End configurations.

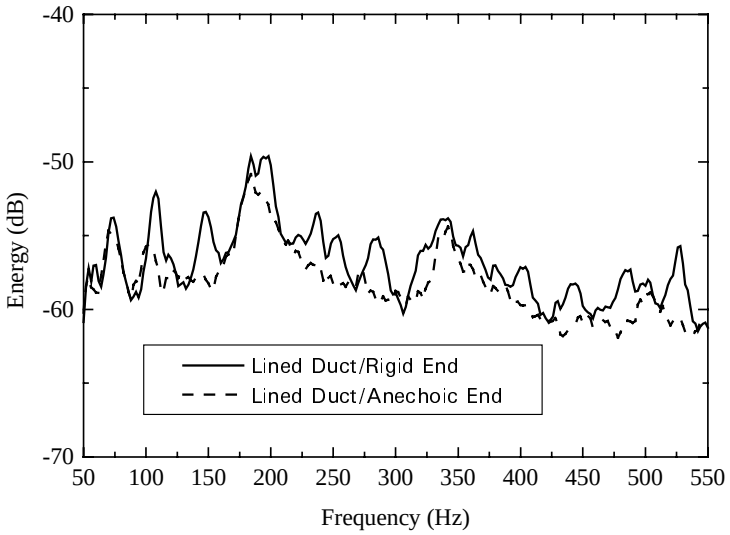

Figure 5.7 Comparison of acoustic energy vs. frequency for Lined Duct/Rigid End and Lined Duct/Anechoic End configurations.

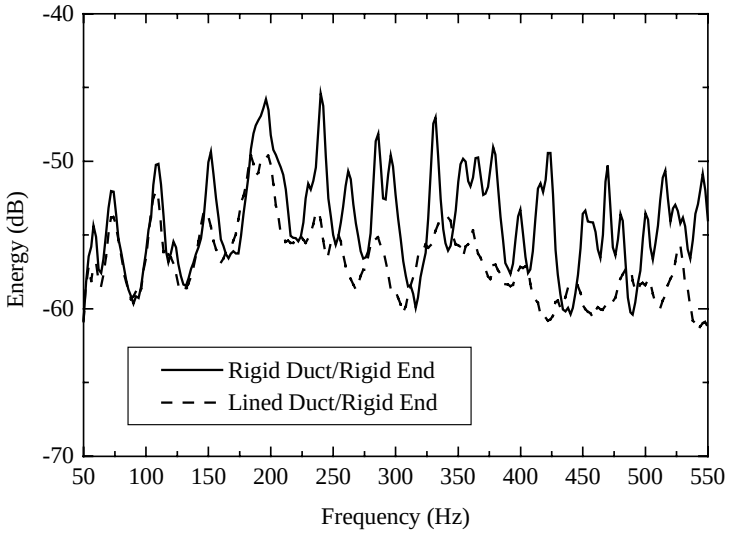

Figure 5.8: Comparison of acoustic energy vs. frequency for Rigid Duct/Rigid End and Lined Duct/Rigid End configurations.

As stated previously, the phase interference between the axially transmitted and reflected waves at the duct termination will result in the formation of a longitudinal standing wave pattern. The previous figures illustrating the results from the modal

analysis revealed that qualitatively the anechoic wedge virtually eliminates the standing wave pattern associated with the longitudinal modes above 122 Hz. The measured properties of the standing wave can be used to determine the power reflection coefficient [80]. It quantitatively predicts the amount of energy reflected relative to the total incident energy impinging on a surface and is illustrated as a function of frequency in Figure 5.9. Accordingly, the power reflection coefficient can be used to rate the efficiency of the anechoic wedge relative to minimizing the longitudinal standing wave pattern in the duct. These measurements are at frequencies below the frequency corresponding to the first transverse mode. It is established by calculating the relative maximum and minimum of the incident pressure wave for the anechoically-terminated, rigid walled duct. Assume the pressure at a point, x, in the duct of length L is denoted by

$$p = A\exp(j\omega t + k(L-x)) + B\exp(j\omega t - k(L-x)) \tag{5.2}$$

where A and B are the incident and reflected wave amplitudes. The amplitude at a pressure antinode is A+B, and the amplitude at a node is A-B. The ratio of pressure amplitude at an antinode to that at a node is the standing wave ratio and is defined as

$$SWR = \frac{A+B}{A-B} \tag{5.3}$$

which can be rearranged to provide

$$\frac{B}{A} = \frac{SWR-1}{SWR+1} \tag{5.4}$$

Thus, measurement of the SWR by probing the length of the duct with a microphone array, as done in the modal analysis, yields a value for B/A, from which the power reflection coefficient is

$$R = \left|\frac{B}{A}\right|^2 \tag{5.5}$$

In Figure 5.9, it is observed that generally the power reflection coefficient decreases as the frequency increases. At 150 Hz less than 22% of the incident power is reflected. This observation confirms that the anechoic wedge minimizes the longitudinal standing wave pattern in the duct for the test frequency range (f>150 Hz).

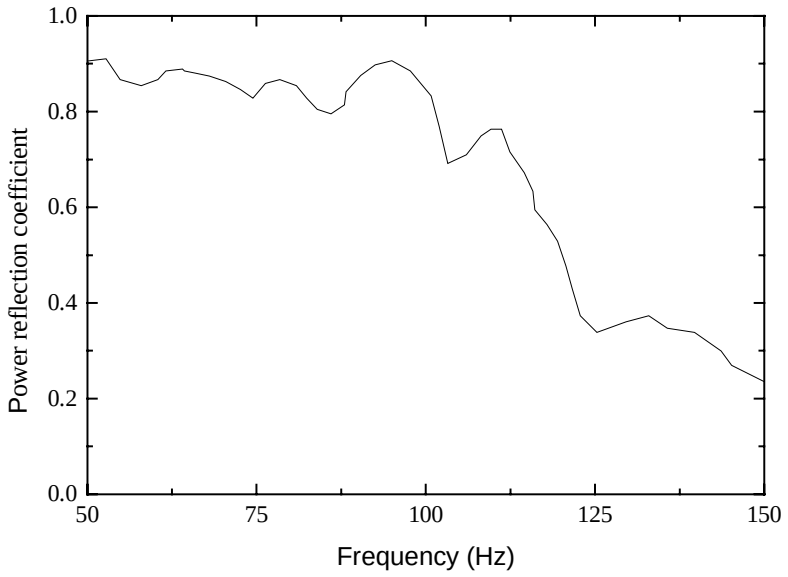

Figure 5.9: Power reflection coefficient vs. frequency for the anechoically-terminated, rigid duct.

5.4 Smart Foam Module Properties & Construction

The design of the smart foam modules for the following duct acoustic control experiments were governed by power amplifier specifications, space constraints within the duct, observations from the preliminary radiation control experiments and results from numerical simulations of the actuator response. For clarity, this information is summarized below:

(1) Three Polytechnic© amplifiers are available. Each amplifier can drive a PVDF actuator having a 130 nF capacitance with 300 V_{rms} up to approximately 1000 Hz.

(2) Width of smart foam modules limited to 6.0 in., which is the width of the duct.

(3) To minimize nonlinear behavior and increase audibility, the curved PVDF actuator surface may be etched or divided into multiple transducers. Neighboring cells are driven with a voltage of opposing polarity. (This is only necessary if using one continuous PVDF film over a foam surface made up of a series of transducers of

opposing physical polarity, as seen in the piston radiation control application of Chapter 2).

(4) A PVDF actuator configured as a half-cylinder proved to be a very efficient actuator and it's sound output increases as the PVDF radius increases (see Chapter 4).

(5) A thin bonding layer should be used to reduce nonlinear behavior, increase PVDF audibility and minimize weight of actuator (see Chapter 2).

(6) Fixed boundary conditions increase PVDF actuator vertical displacement and results in an increase in the sound output (see Chapter 4).

(7) Smart foam module may be framed or placed within rigid support to increase low-frequency radiation efficiency (see Chapter 3).

With regard to comments (1), three Polytechnic amplifiers were available to provide the excitation voltage for an array of smart foam actuators. The maximum power output of the amplifier was used to extrapolate the maximum capacitance allowable for each smart foam actuator. Owing to the necessity to manufacture smart foam modules with the largest PVDF radius possible but not violate the power limitations of the threes amplifier, it was possible to manufacture an array of six smart foam modules and wire every two actuators in phase A single smart foam module has a capacitance of approximately 65 nF. As stated in comment (2), each smart foam is configured to have a width of 6.0 inches in order to cover the entire width of the duct bottom wall. In reference to comments (3) and (4), a single PVDF actuator was embedded within each smart foam module. This step removes the necessity to etch between neighboring transducers because there is only one actuator. Since the foam has a thickness of 2.0 in., the actuator is configured as a half-cylinder with a 2.0 in. radius which is the largest that can be used. A light, spray adhesive is used to embed the PVDF within the foam, as suggested in comment (5). With regard to comment (6) and (7), a 4.0 in. (width) x 2.0 in. (thickness) x 6.0 in. (length) frame composed of balsa wood encased each smart foam actuator. This frame has longitudinal stiffeners which are used to fix the periphery of the PVDF which increases the sound output of the actuator. Photographs of the top and bottom surface of one of the smart foam modules, as used in the duct noise control experiments, appear in Figures 5.10.

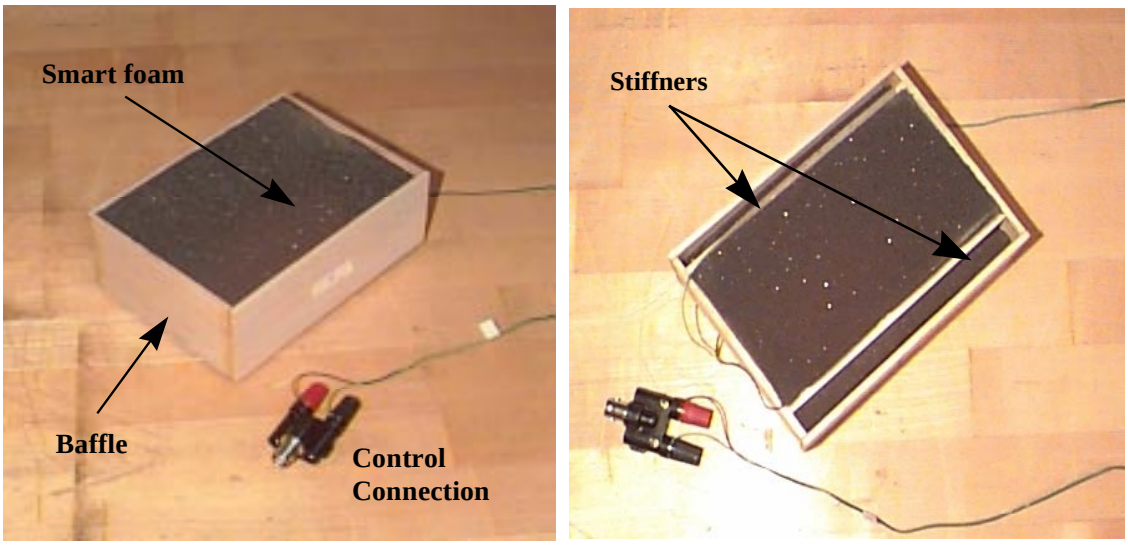

Figure 5.10: (a) Top view of single smart foam module used in duct experiments (b) Bottom view of single smart foam module used in duct experiments.

5.5 Duct Acoustic Control Experimental Setup & Procedure

A MIMO feedforward Filtered-x LMS control algorithm is implemented to perform active control of sound propagation in the duct. The experimental setup in Figure 5.12, illustrates the duct with the side wall removed to reveal the arrangement of the components in the interior of the cavity. As stated previously, the noise source is located in the upper left corner of the duct. This position is chosen so that the transverse acoustic modes are excited and propagate down the length of the duct toward the anechoic termination. Three arrays of sixteen microphones are located at 9.0 in. increments from the noise source. These microphones are referred to as observation microphones because they measure the pressure "upstream" of the control actuators before and after control. Three arrays of sixteen microphones are located at 9.0 in. increments from the anechoic termination. These observation microphones measure the pressure "downstream" of the control actuators before and after control. The vertical distance between neighboring microphones in each array is 2.375 in., this distance allows the microphones to be evenly distributed along the height of the duct. Certain microphones on array 4 are used as error microphones and will be identified as the experimental results are presented. The center of the array of six smart foam actuators (the total length of the actuator array is 2.0 ft.) are located on the bottom wall of the duct and positioned at a 4.0 ft. distance from the noise

source. Similarly, the center of the actuator array is 4.0 ft. from observation microphone array 4, which contains the error sensors. The remaining exposed rigid bottom wall of the duct is carpeted with homogeneous partially-reticulated foam. A time domain, digital control algorithm is provided by DIGIWARE©, an applications development system for active sound and vibration control developed by Digisonix Inc. which runs under Microsoft Windows [81]. The PC software of the system consists of two main divisions: (1) *Composer*, a Digisonix program functions as an editor for configuring DSP algorithms and defining hardware arrangements; (2) *Conductor*, a Digisonix program that performs as both a monitor and control shell for DSP devices. Before and after control, the output of every microphone in the experimental setup is recorded using a LABVIEW© data acquisition program. A detailed discussion of the control code follows.

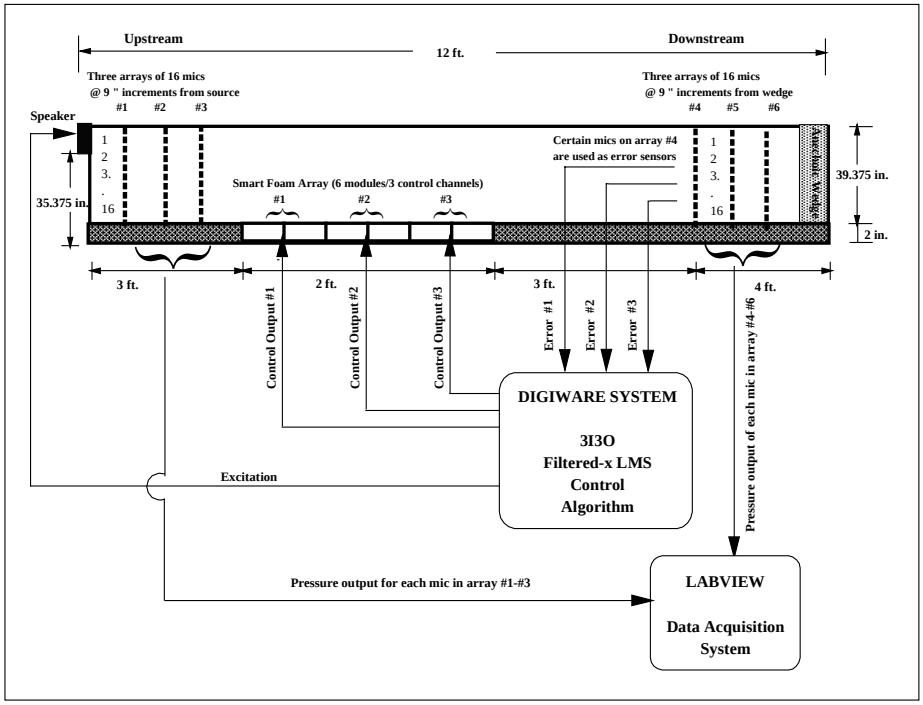

Figure 5.11: Experimental setup for duct acoustic control experiment.

A schematic of the implementation of the feedforward, Filtered-x LMS control approach for the duct acoustic control application is presented in Figure 5.12. Again, the control algorithm is implemented within the DIGIWARE system which may be instructed

to deal with a variety of control schemes, however, a 3I3O control setup is used as an example. For this particular setup, the goal is to minimize the pressure at three error microphones associated with microphone array 4, as shown in Figure 5.13(a), while providing global sound control downstream of the control actuators. A photograph of the smart foam actuator array positioned on the bottom wall of the duct is presented in Figure 5.13(b). The excitation or reference signal is provided by a signal generator internal to the DIGIWARE© system and drives the acoustic speaker with either harmonic or broadband noise. The output at each error microphone is the sum of the signal due to the primary source acting alone and an output due to each of the actuators. Prior to implementing control, during a system identification process, the transfer functions, C_{lm}, corresponding to the m^{th} control actuator input and the output at the l^{th} error sensor is established. In the Filtered-x control algorithm, the excitation is "fed forward" and filtered by these control path transfer functions to formulate corresponding filtered-x signals. The control input to the m^{th} control actuator is defined by filtering the reference signal using an adaptive FIR (finite impulse response) controller, A_m. The approach relies on constructing a quadratic cost function by squaring the moduli of the error sensor outputs and then employing gradient search methods to locate the unique minimum of the cost function. Specifically, each coefficient is adjusted at every sample time by an amount proportional to the negative instantaneous value of the gradient. It is important to note that if the reference signal is at least partly correlated (i.e. contains the same frequency components) with the sensor output due to the primary source operating alone, it is possible to reduce the value of the error by driving the control actuators with a filtered version of the reference signal. This is the essence of the filtered-x, LMS (least mean square) algorithm [82].

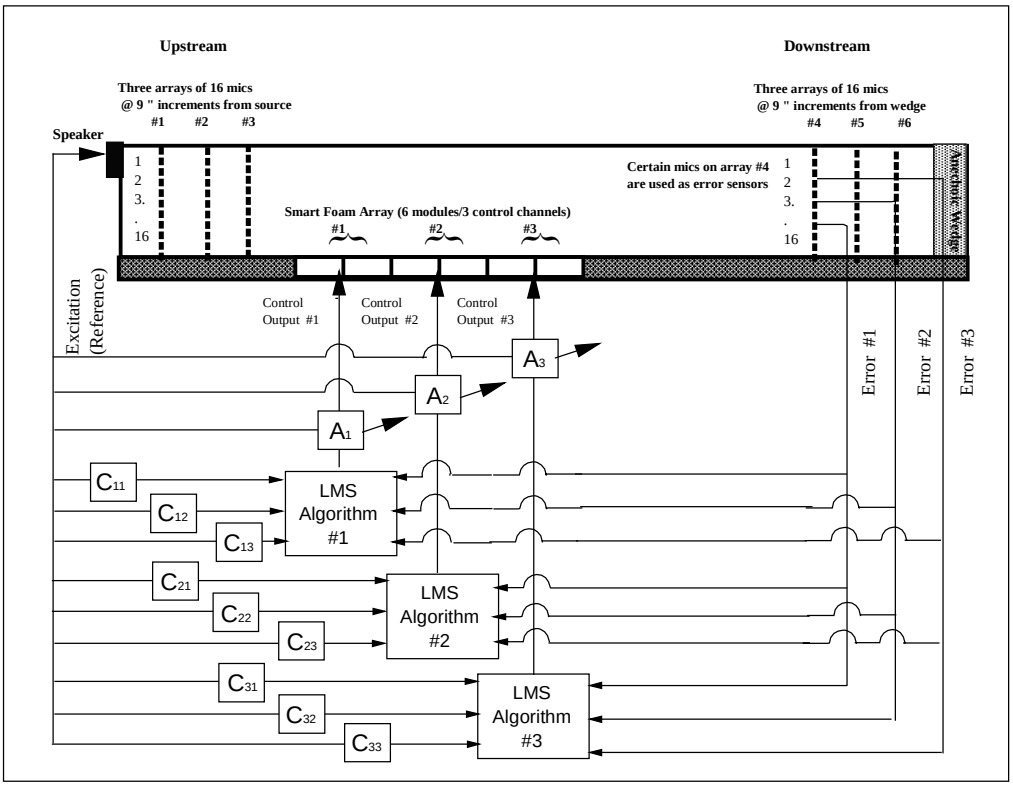

Figure 5.12 MIMO Feedforward filtered-x control algorithm.

(a) (b)

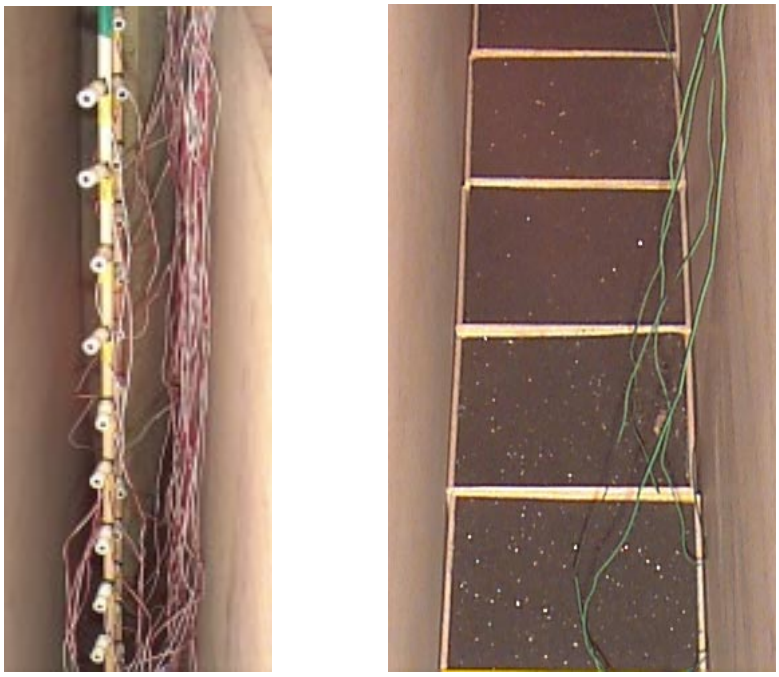

Figure 5.13. (a) Array of observation microphones located in the cross section of the duct. (b) Array of smart foam actuators on the bottom wall of the duct

5.6 Experimental Duct Acoustic Control Results

5.6.1 Acoustic Characteristics of Smart Foam Actuators within Enclosure

As noted in the previous smart foam noise control applications in this study, it is important to investigate the actuator acoustic response prior to implementing control because it indicates the actuator's sound reduction capability in terms of identifying the maximum controllable sound level. In the present experiment, smart foam control channel 1 is used as a noise source (i.e. the acoustic disturbance speaker is inactive). The actuator is consecutively excited with input voltages of 75, 150, and 300 V_{rms} and the sound pressure is recorded by microphone array 4 at the excitation frequency and it's first and second harmonic frequencies. The mean square pressure output of the microphones associated with array 4 are then averaged and converted to sound pressure level in dB. The experiment is performed for excitation frequencies of 184 Hz, 342 Hz and 504 Hz which correspond to the first, second and third transverse modes of the duct, respectively,

as listed in Table 5.1. In the next section, acoustic control results within the duct will be presented at these frequencies.

Figure 5.14(a) illustrates the sound pressure level generated by a 184 Hz excitation frequency. The maximum possible sound pressure level radiated by the actuator at 184 Hz is 60 dB, corresponding to an input voltage of 300 V_{rms} . Moreover, the results show that the sound pressure level increases by about 6.0 dB each time the input voltage is doubled. This proves that the actuator is linear with respect to voltage. Information concerning the linearity of the smart foam actuator with respect to frequency is also given in Figure 5.14(a). As stated in Chapter 2, any frequency content from the harmonics of the drive frequency in the acoustic response of the actuator is considered nonlinear behavior and should be avoided or minimized. Nonlinear effects are observed by comparing the sound pressure levels at 184 Hz with it's first and second harmonic at a particular input voltage. It is evident that the sound levels at the harmonics increase as the input voltage increases. Considering an input voltage of 300 V_{rms}, the sound level at the drive frequency is 60 dB and the sound pressure levels related to the first and second harmonics are 38 dB at 368 Hz and 27 dB at 552 Hz, respectively. Note that the sound pressure level at the harmonics are over 20 dB below the sound pressure level of the drive frequency. indicating that the nonlinear behavior of the actuator is minimal. Figure 5.14 (b) presents the sound pressure level related to a 342 Hz excitation frequency. The maximum possible sound pressure level radiated by the actuator at 342 Hz is 75 dB, corresponding to an input voltage of 300 V_{rms}. Figure 5.14(c) presents the sound pressure level related to a 504 Hz excitation frequency. The maximum possible sound pressure level radiated by the actuator at 504 Hz is 80 dB. Observing the sound pressure levels at 342 Hz and 504 Hz as the input voltage is increased, further reveals the linearity of the actuator with respect to voltage. Furthermore, noting the contribution of the higher-order harmonics at each frequency shows that there is minimal nonlinear behavior at these frequencies.

This experiment is repeated at the same frequencies (i.e. 184 Hz, 342 Hz and 504 Hz) using channel 2 and channel 3 as noise sources, respectively. The results

showed that each of these control channels behave linearly with respect to input voltage and exhibited minimal nonlinear behavior with respect to frequency.

(a)

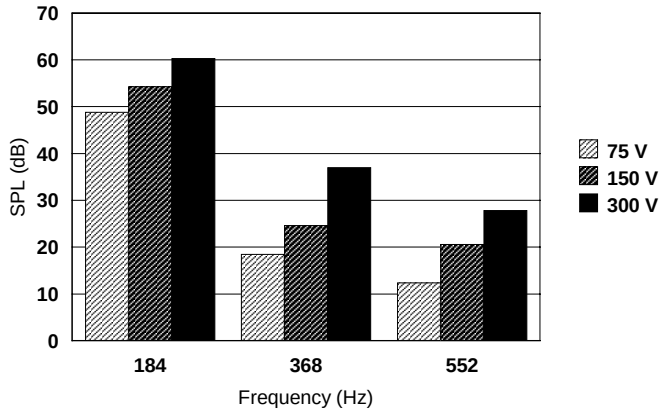

(b)

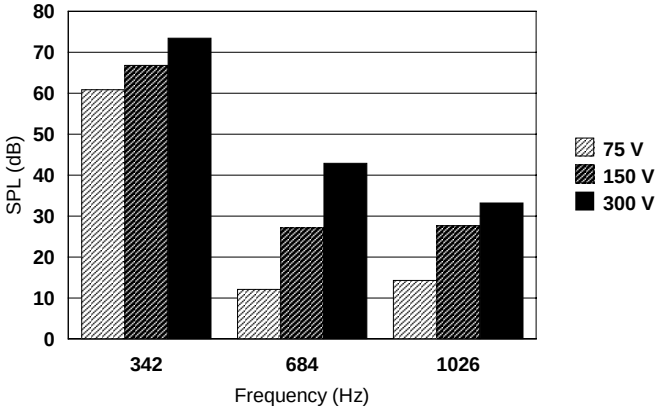

(c)

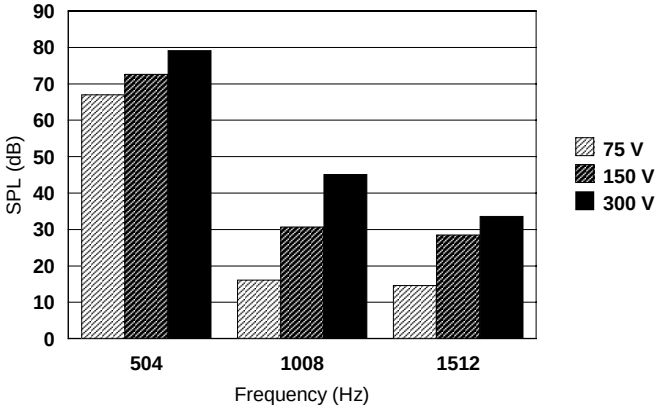

Figure 5.14: Smart foam acoustic response vs. voltage input (a) at harmonics of 184 Hz (b) at harmonics of 342 Hz (c) at harmonics of 504 Hz.

5.6.2 *Harmonic Control: 2I2O & 3I3O Cases @ 184 Hz (Transverse mode 1)*

In this experiment, the acoustic speaker is driven at 184 Hz which corresponds to the first transverse mode of the anechoically-terminated, lined duct. Recall, the modes and corresponding resonance frequencies of the duct are listed in Table 5.1 and the experimental setup is shown in Figure 5.11. A sampling frequency of 800 Hz and four control filter coefficients are used in all noise control experiments performed at 184 Hz.

The "global" sound distribution *upstream* and *downstream* of the control actuators is of interest as the sound pressure is minimized at a number of discrete points associated with microphone array 4. The global *upstream* sound levels are calculated by longitudinally averaging the mean square pressure values at microphone arrays 1-3 and then converting to dB. This yields sixteen unique values corresponding to each of the sixteen transverse positions of the duct cross section. Similarly, the global *downstream* sound levels are calculated by longitudinally averaging the mean square pressure values at microphone arrays 4-6 and then converting to dB. (In the interest of completeness, the appendix of this dissertation contains the raw data illustrating the SPL variation relative to longitudinal distance for each microphone array in the experimental setup). To study the efficiency of smart foam in providing global sound reduction, the global sound levels are plotted relative to the 16 transverse duct positions for three duct configurations:

(1) Untreated Duct (*Anechoically-terminated, rigid walled duct*).

(2) Passive Control (*Foam-lined duct with inactive smart foam array*).

(3) Active/Passive Control (*Foam-lined duct with active smart foam array*).

In the following tests, various actuator and error sensor configurations are studied. Note that the "modal order" corresponds to the number of interfering plane waves necessary to formulate a particular acoustic mode shape. It is suspected that the number of error sensors, L, and control actuators, M, should be equal to the modal order to gain significant global sound attenuation. The control system dimensions can be defined with the indices (L,M). The placement of the three channel smart foam array is fixed as shown in Figure 5.11 for all tests. However, the number of "activated" control channels can vary. It is further suspected that error microphone locations which correspond to the maximum

sound level of the transverse mode shape in the enclosure will generate the highest global sound attenuation in the duct. These assumptions shall be investigated for validation in the following tests.

In an initial experiment, the pressure is arbitrarily minimized at microphone 1 and microphone 16 and smart foam control channel 2 and channel 3 are employed as actuators (see Figure 5.11). The global upstream sound pressure level is plotted in Figure 5.15(a) for the three cases listed above. Note the similarity of the mode shape for the untreated duct and passive control case. This is attributed to the virtual coincidence of the first transverse resonance frequencies for each unique system (see Table 5.1). It is interesting that some active/passive attenuation is achieved upstream of the control actuators even though the pressure is not minimized in this area of the duct. Considering the average sound attenuation along the transverse cross section of the duct, approximately 5.0 dB active/passive sound reduction is achieved. Even though, some passive sound reduction is gained near the bottom wall of the duct at microphones 8-16, on an average level the amount of passive reduction is less than 1.0 dB. This poor performance of the liner in generating global upstream passive sound reduction at 184 Hz may be explained in terms of the acoustic wavelength of the excitation. The minimal passive sound attenuation is attributed to the short longitudinal distance traveled by the low-frequency disturbance to the upstream measurement points relative to it's wavelength.

The global downstream sound pressure level is shown in Figure 5.15(b). A global active/passive sound reduction of 12.2 dB and 8.72 dB is obtained at error microphone 1 and error microphone 16, respectively. This corresponds to a global downstream active/passive reduction of 5.0 dB, with approximately 1.0 dB contributed by the passive foam liner. As in the upstream case, the passive sound attenuation is concentrated at microphones 8-16, which are located near the bottom wall of the lined duct. Note that the upstream and downstream global sound reduction is the same. Each smart foam control channel used approximately 200 V_{rms} to achieve these results.

An alternative 2I2O harmonic control configuration is implemented at 184 Hz in the following experiment. As in the previous case, only smart foam control channel 2 and channel 3 are employed as actuators, however, the pressure is minimized at microphone 1

and microphone 8 within downstream microphone array 4. Observe that these microphone locations correspond to the section of the mode shape that provides maximum sound levels. The global sound pressure level, related to the three upstream microphone arrays, is plotted in Figure 5.16(a). A similar global active/passive attenuation of 5.0 dB is achieved upstream of the control actuators, as noted with the previous error sensor configuration. The global sound pressure level measured at the downstream microphone arrays is shown in Figure 5.16(b). At the error sensors, microphone 1 and microphone 8, a 25.2 dB and 6.45 dB reduction is gained, respectively. This corresponds to a global downstream active/passive reduction of 13.0 dB Each smart foam control channel is driven by approximately 215 V_{rms} to achieve these results. It is observed, by comparing Figures 5.15(b) and 5.16(b), that increased global sound attenuation is gained downstream by locating both error sensors in the upper half of the duct. This is attributed to the fact that the pressure is highest near the top wall of the duct which is not treated with an acoustic foam liner.

Harmonic control at 184 Hz implementing a 3I3O control approach is investigated. Note that the dimensions of the control system (3,3) exceeds the modal order which has a value of 2 For this setup, microphone 1, 8 and 16 on array 4 are utilized as error sensors. These locations correspond to points of maximum pressure relative to the mode shape. All three smart foam control actuators are excited. The global sound pressure levels measured by the upstream microphone arrays are plotted in Figure 5.17(a). The global upstream passive attenuation is about 1.0 dB, as in the other control schemes presented at 184 Hz. However, the upstream active reduction achieved with the current control setup is only about 1.0 dB, which is less than the reduction achieved using previous control schemes

The global sound pressure levels measured by the downstream microphone arrays are shown in Figure 5.17(b). The active/passive sound reduction at the error sensors are 19.6 dB, 12.7 dB and 8.5 dB, respectively. The global active/passive sound attenuation in this region is approximately 13.0 dB, with minimal passive attenuation. The control voltages used for channel 1 and 2 are approximately 200 V_{rms}. while the third channel used much less. The results infer that to control the first transverse acoustic mode which

is constructed from the interference of two uniquely phased sound waves, only two control channels are needed.

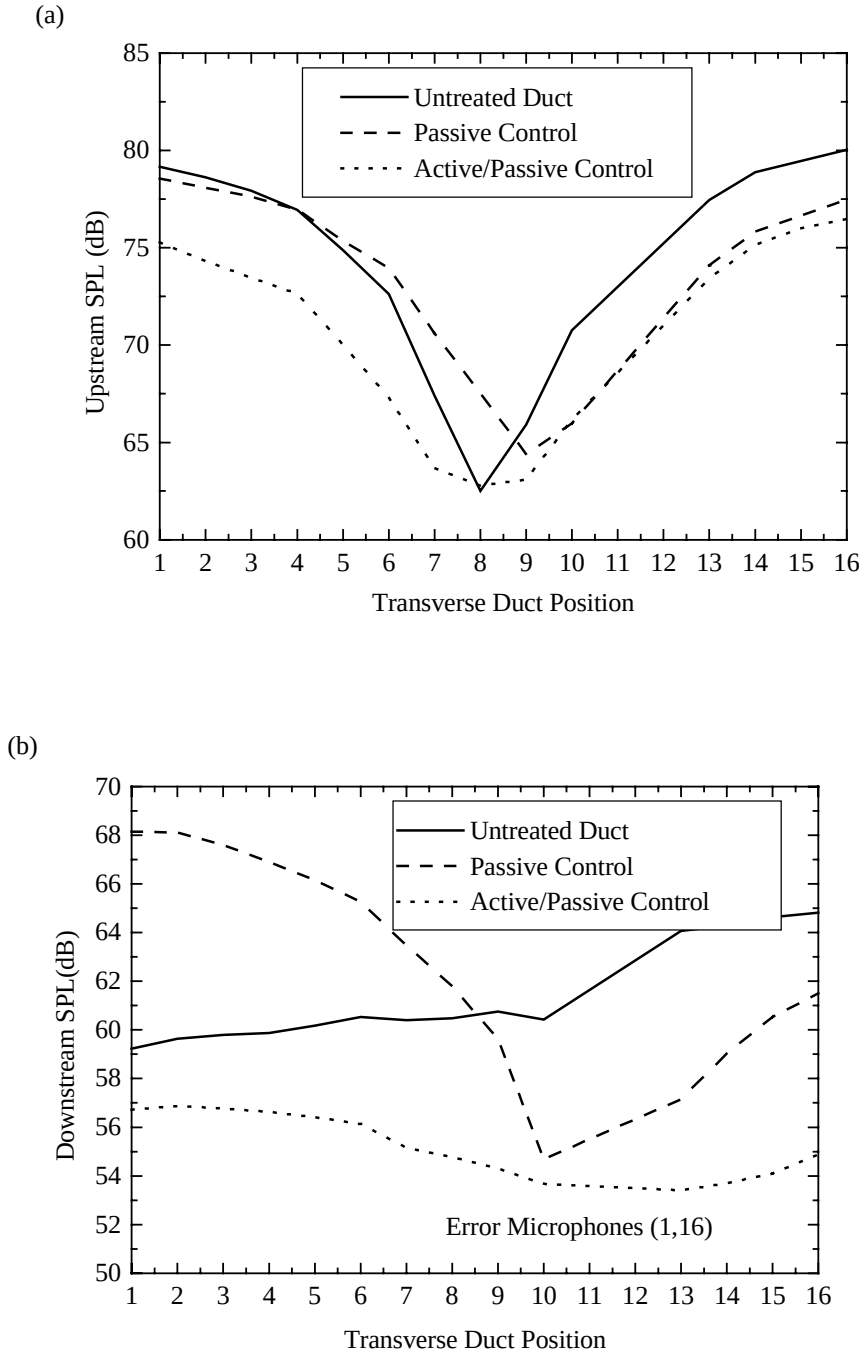

Figure 5.15: 2I2O Harmonic Control at 184 Hz with error microphones 1,16 (a) *Upstream* SPL vs. Transverse duct position (b) *Downstream* SPL vs. Transverse duct position.

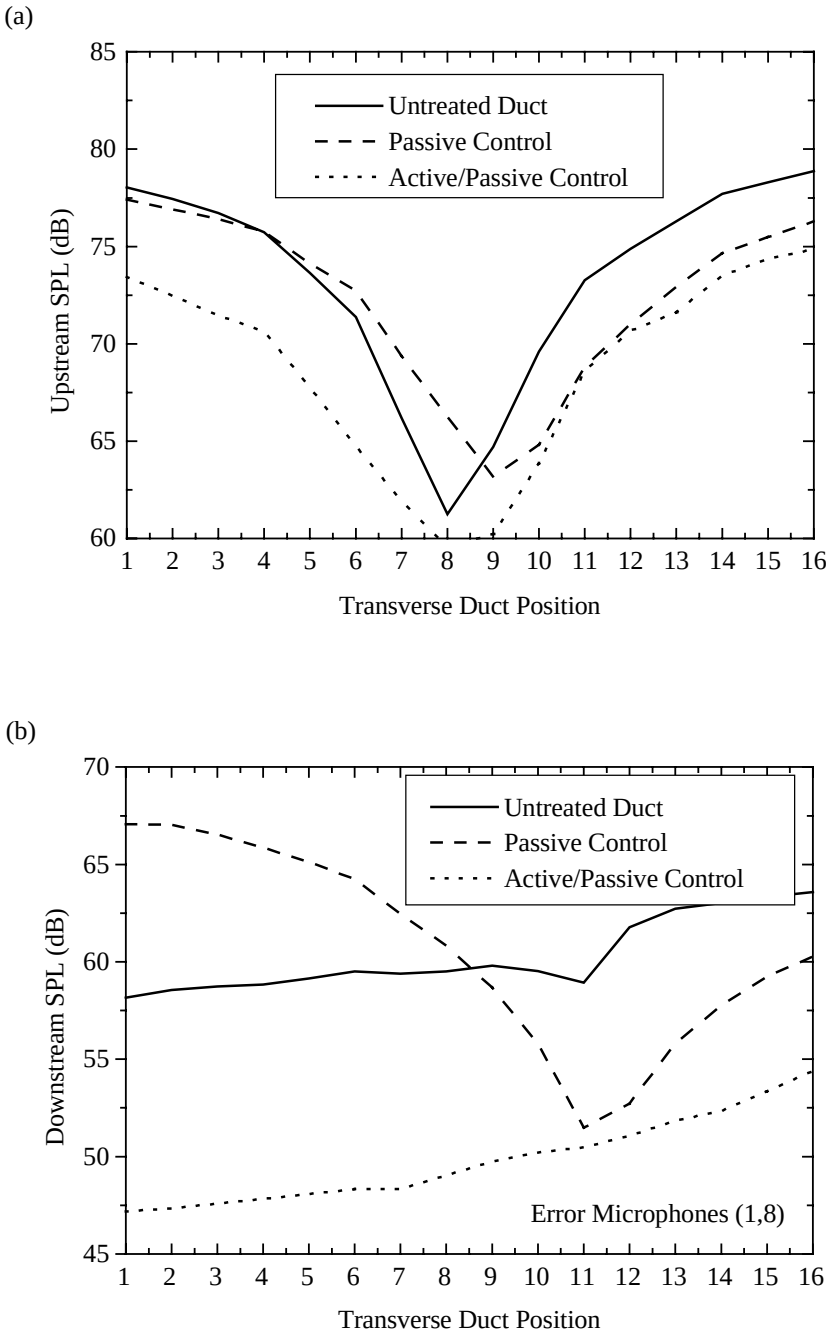

Figure 5.16: 2I2O Harmonic Control at 184 Hz with error microphones 1,8 (a) *Upstream* SPL vs. Transverse duct position (b) *Downstream* SPL vs. Transverse duct position.

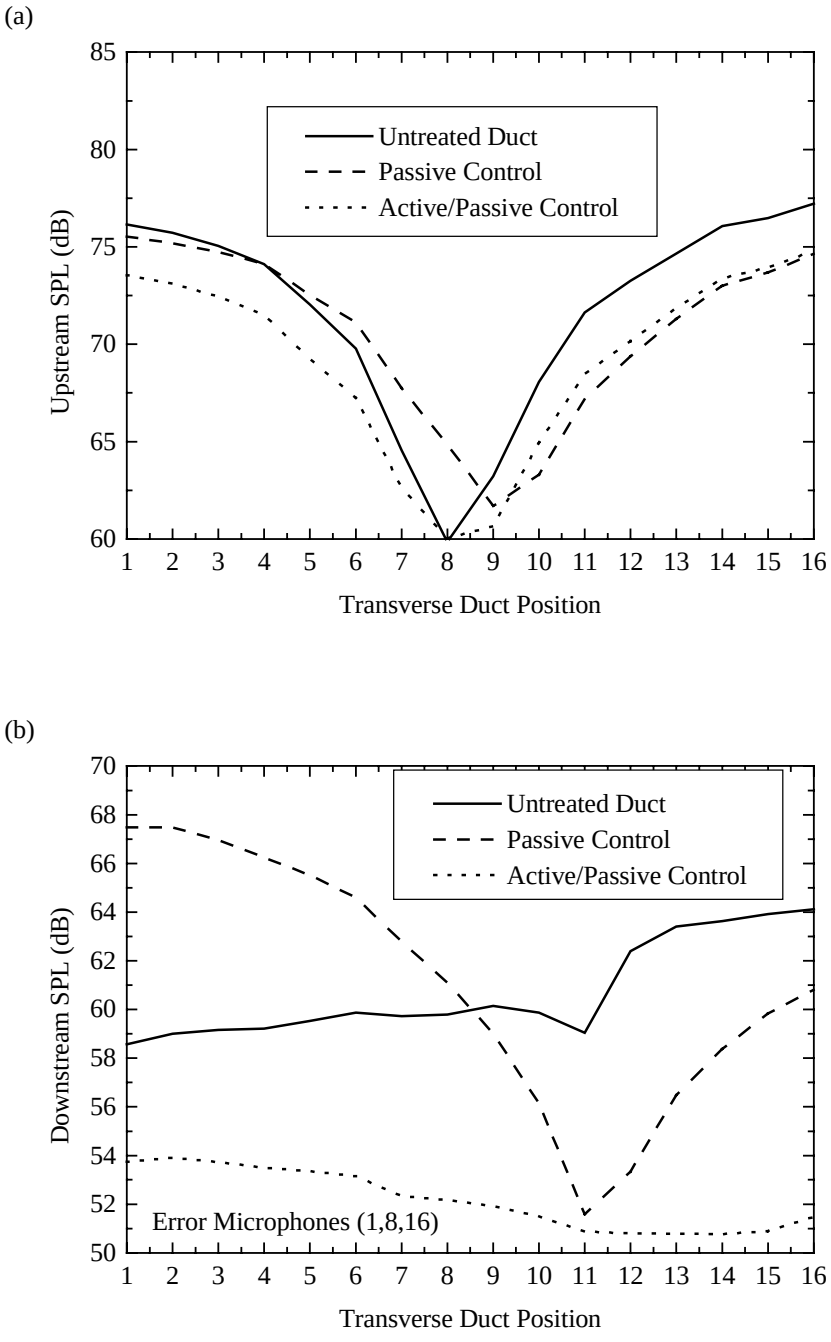

Figure 5.17: 3I3O Harmonic Control at 184 Hz with error microphones 1,8,16 (a) *Upstream* SPL vs. Transverse duct position (b) *Downstream* SPL vs. Transverse duct position.

The previous control results imply that when minimizing the acoustic response within the duct at 184 Hz, corresponding to the first transverse mode, comparable global downstream noise reduction is achieved with a 2I2O or 3I3O control setup. Comparing the active/passive curves of Figures 5.16(b) and 5.17(b), it is revealed that a 3I3O control system accounts for more uniform reduction at the downstream sensors, but does not provide increased global downstream sound control. Further confirmation of these observations in evident by viewing the raw data illustrated in Figures A.1-A.3 of the appendix.

5.6.3 *Harmonic Control: 2I2O & 3I3O Cases @ 342 Hz (Transverse mode 2)*

In this experiment, the acoustic speaker is excited at 342 Hz which corresponds to the second transverse mode of the anechoically-terminated, lined duct. A sampling frequency of 1500 Hz and four control filter coefficients are implemented in all control experiments performed at this frequency.

The first 2I2O control scheme arbitrarily minimizes the pressure at microphone 1 and microphone 16 of downstream microphone array 4. Smart foam control channel 2 and channel 3 are employed as actuators. Note that the current control case involves a third order mode and the dimensions of the control system are (2,2). The global upstream sound pressure level is plotted in Figure 5.18(a). Only a minimal amount of global upstream passive attenuation is gained which is about 2.0 dB near the lined bottom wall of the duct. Generally, the passive liner manifests a 4.0 dB increase in global sound level relative to the untreated duct. A further 4.0 dB increase is generated by the addition of active control. The justification for the exacerbation of the upstream sound levels with the addition of passive control may be found in Table 5.1. Compare the second acoustic transverse mode resonance frequencies of an anechoically-terminated, rigid duct and an anechoically-terminated lined, duct which are 356 Hz and 342 Hz, respectively. The effect of the liner is to lower the resonance frequency by about 14 Hz.. Thus, the transverse pressure distribution of the untreated duct at 342 Hz does not correspond to a particular resonance frequency of that system. Because the addition of the liner considerably alters the pressure distribution within the duct, an increase in sound levels is

observed at some positions. The increase in sound levels upstream of the control actuators during active control implies that addition of the secondary acoustic control field causes "constructive" interference with the primary acoustic field. The obvious question is at the expense of upstream control spillover, is active sound reduction achieved downstream of the control actuators?

The global sound pressure level downstream of the control actuators is shown in Figure 5.18(b). At error microphone 1 and microphone 16, an active/passive reduction of 3.5 dB and 13.3 dB is yielded, respectively. A global downstream active/passive sound reduction of 5.0 dB is obtained. This corresponds to a passive and active reduction of 1.0 dB and 4.0 dB, respectively. Each smart foam control channel used approximately 150 V_{rms} to achieve these results.

Another 2I2O control setup is performed at 342 Hz and implements microphone 1 and microphone 10 associated with downstream microphone array 4 as error sensors. These positions correspond to maximum sound levels along the mode shape of the anechoically-terminated, lined duct. Again, only smart foam control channel 2 and channel 3 are employed as control actuators. The upstream global sound pressure level is plotted in Figure 5.19(a). Similar upstream active/passive control spillover is observed, as in the previous 2I2O control scheme.

The global downstream sound pressure levels of the lined duct are shown in Figure 5.19(b). An active/passive sound reduction of 7.2 dB and 29.4 dB is obtained at the error microphones, respectively. This corresponds to a 6.0 dB global downstream active/passive attenuation, with minimal passive sound reduction observed. Smart foam control channel 1 and channel 2 are driven by approximately 150 V_{rms}, respectively, in order to minimize the pressure at the error sensors.

It has been shown that satisfactory global downstream sound reduction can be achieved implementing a 2I2O control system to minimize the second propagating transverse mode of the duct. The next step is to compare these control results with the performance offered by a 3I3O control .setup, since this is a third order mode.

The final experimental control configuration at 342 Hz implements a 3I3O control scheme. Microphones 1, 8 and 16 on downstream microphone array 4 acts as the error

sensors in this test setup. These positions correspond to points of maximum sound levels relative to the third transverse mode shape of the anechoically-terminated, lined duct. All three smart foam control channels are active in this experiment. The global sound pressure level upstream of the control actuators is plotted in Figure 5.20(a). Active/passive control generates an increase in the sound levels in this region of the duct. The global downstream sound pressure is illustrated in Figure 5.20(b). An active/passive sound reduction of 18.0 dB, 21.0 dB and 20.0 dB is obtained at error microphone 1, 8 and 16, respectively. This corresponds to a l9 dB active/passive reduction, with only 1.0 dB reduction attributed to passive control. Each smart foam channel is driven by about 150 V_{rms} while minimizing the downstream sound pressure at each error sensor.

Some important observations can be made by a comparative analysis of the previous duct acoustic control results performed at 342 Hz which corresponds to the second transverse acoustic mode of the duct. Studying the results achieved by the 2I2O and 3I3O control approaches indicates that in terms of global attenuation of the second mode, a 3I3O controller gives superior results. However, it is noted that considerable downstream reduction is achieved at the expense of increasing the sound levels upstream of the smart foam array. Further confirmation of these observations in evident by viewing the raw data illustrated in Figures A.4-A.6 of the appendix.

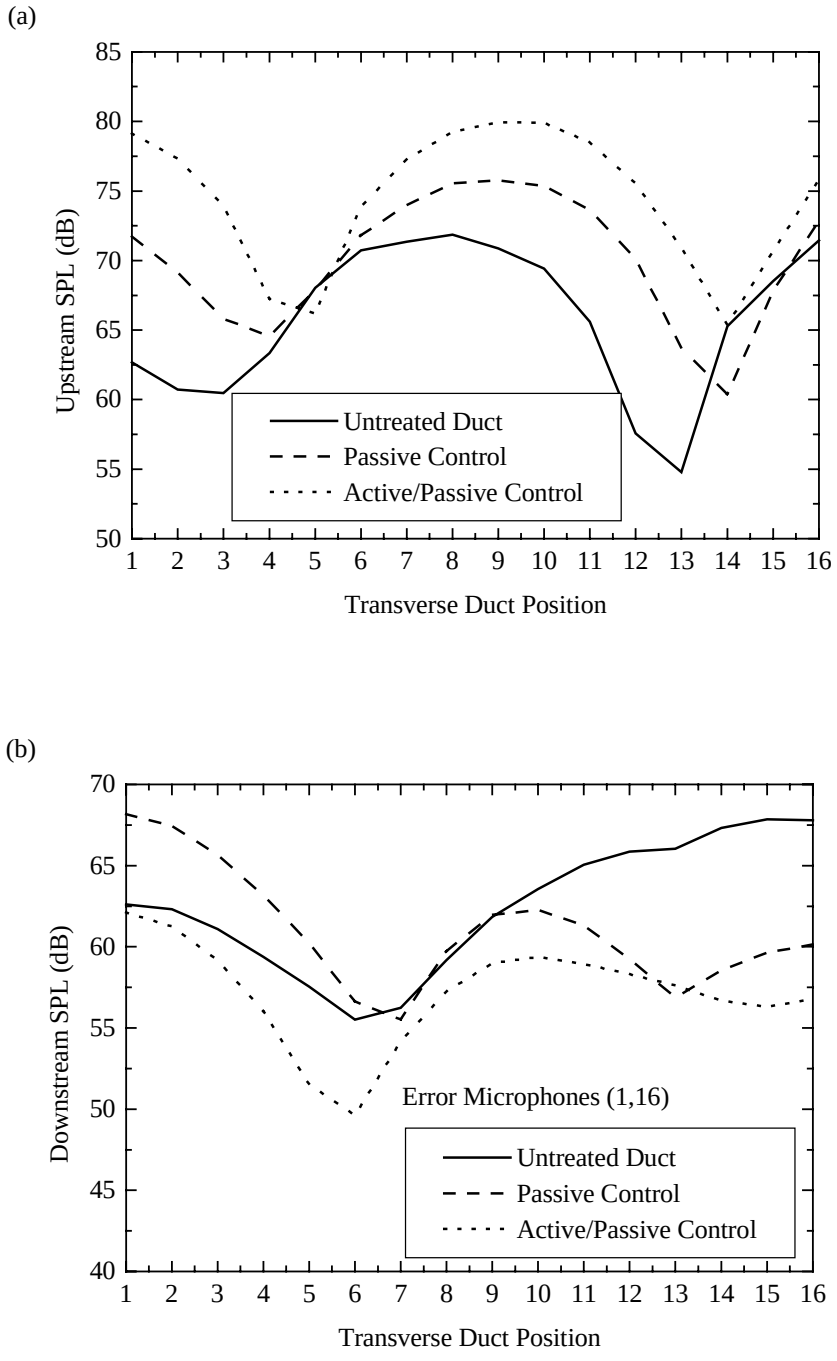

Figure 5.18: 2I2O Harmonic Control at 342 Hz with error microphones 1,16 (a) *Upstream* SPL vs. Microphone number (b) *Downstream* SPL vs. Microphone number.

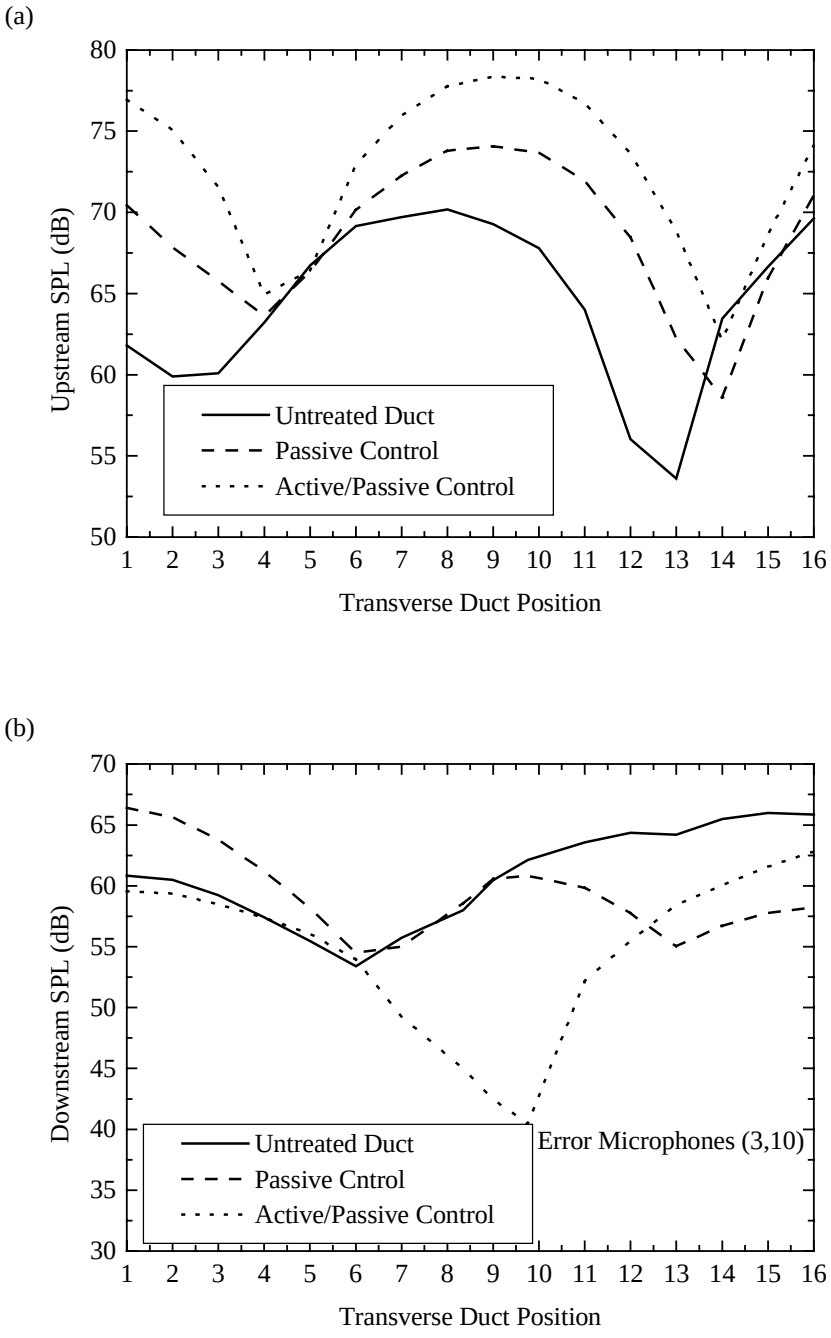

Figure 5.19: 2I2O Harmonic Control at 342 Hz with error microphones 3,10 (a) *Upstream* SPL vs. Microphone number (b) *Downstream* SPL vs. Microphone number.

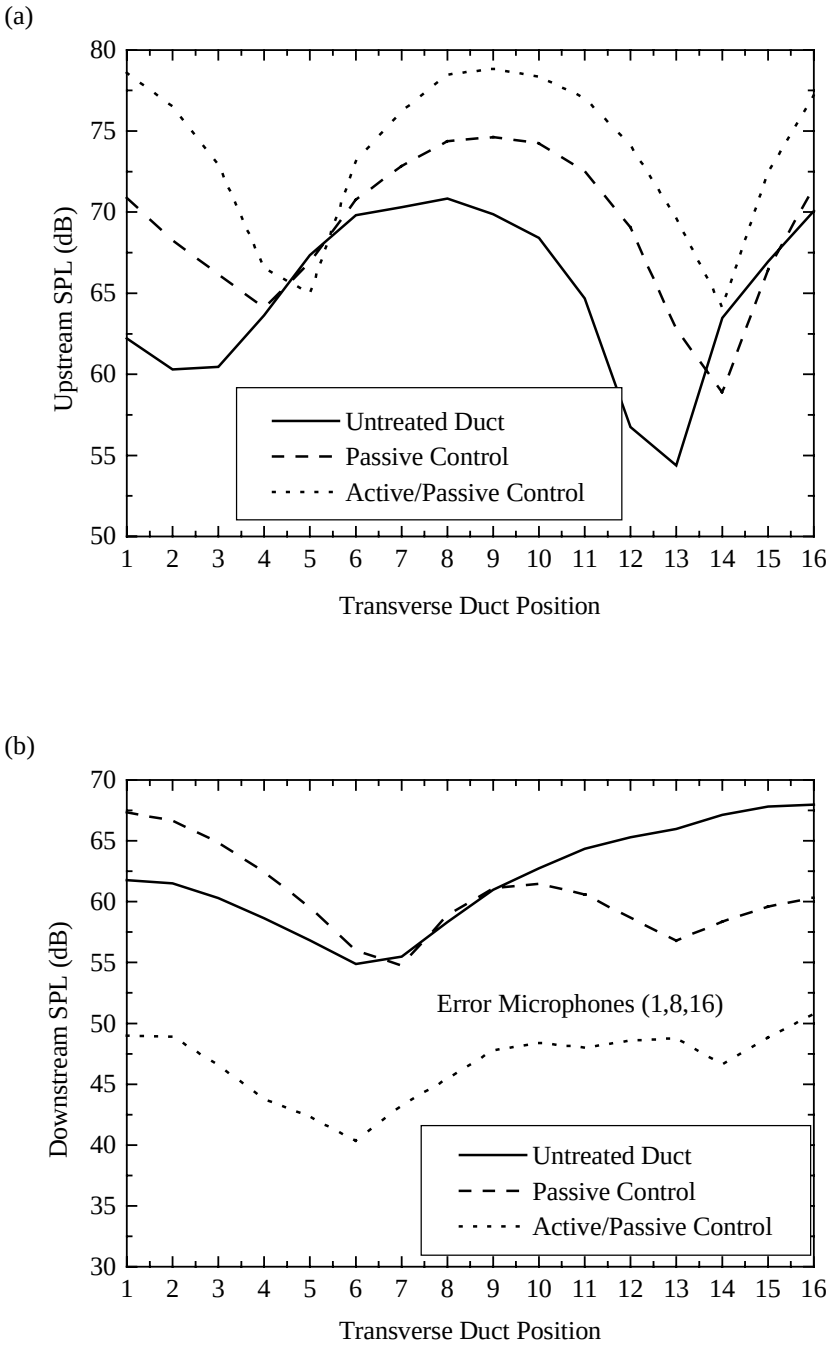

Figure 5.20: 3I3O Harmonic Control at 342 Hz with error microphones 1,8,16 (a) *Upstream* SPL vs. Microphone number (b) *Downstream* SPL vs. Microphone number.

5.6.4 *Harmonic Control: 3I3O & 4I3O Cases @ 504 Hz (Transverse mode 3)*

The acoustic speaker of the duct is excited at 504 Hz, in this experiment, which is associated with the third transverse mode of the anechoically-terminated, lined duct A sampling frequency of 2000 Hz and four control filter coefficients are used in all harmonic control experiments performed at this frequency.

The pressure is minimized at microphone 1, 8, and 16 and all three smart foam control channels are utilized in the control approach. The global upstream sound pressure level is plotted in Figure 5.21(a). It is observed that the upstream sound levels increase greatly with the addition of active/passive control. Again, the justification for the exacerbation of the upstream sound levels with the addition of passive control may be found in Table 5.1. Note that the third transverse mode resonance frequencies of an anechoically-terminated, rigid duct and an anechoically-terminated, lined duct are at 526 Hz and 504 Hz, respectively. The effect of the liner is to lower the resonance frequency by about 22 Hz.. Thus, the transverse pressure distribution of the untreated duct at 504 Hz does not correspond to a particular resonance frequency of that system. Because the addition of the liner considerably alters the pressure distribution within the duct, an increase in sound levels is observed at some positions. The increase in sound levels upstream of the control actuators during active control implies that addition of the secondary acoustic control field causes “constructive” interference with the primary acoustic field.

The global downstream sound levels are illustrated in Figure 5.21(b). Note that an active/passive sound reduction of 8.0 dB, 4.0 and 11.0 dB is obtained at the error microphones, respectively. In spite of this, there is a global 5.0 dB increase in the sound levels during control due to spillover that occurs away from the microphone positions where the pressure is minimized. At these points the spillover is due to the constructive interference between the primary acoustic field and the acoustic field generated by the control actuators. In this test, each smart foam control channel used approximately 82 V_{rms} during control.

In light of the poor global control performance offered by a 3I3O controller, the final experiment related to control of the third transverse acoustic mode at 504 Hz

employs a 4I3O control setup, by adding an extra error sensor to the configuration. The configuration incorporates microphone‘s 1, 6, 11 and 16 in array 4 as error sensors in an attempt to obtain global downstream control. All three smart foam actuators are used as control actuators. The global upstream sound pressure levels are illustrated in Figure 5.22(a). Similar upstream control spillover is observed as in the previous 3I3O control scheme at 504 Hz. The downstream control results are shown in Figure 5.21(b). An active/passive sound reduction of 10.0 dB, 8.0 dB, 10.0 dB and 5.0 dB is obtained at the four error microphones, respectively. This corresponds to a global downstream sound attenuation of 9.0 dB, with minimal attenuation offered by the passive liner. Each smart foam control channel used approximately 154 V_{rms} during control.

Some important general observations are illustrated by comparison of the experimental results at 504 Hz which corresponds to the third transverse mode of the anechoically-terminated lined duct. Implementing a 3I3O control scheme offered satisfactory sound reduction at the error sensors but spillover was noted at the uncontrolled microphone positions. Comparatively, a 4I3O control scheme prove that minimizing the pressure at four error points yields global sound reduction (See Figures A.7-A.8 of appendix for the raw data).

All of the previous harmonic control results were performed at resonant frequencies of the anechoically-terminated, foam lined duct. At these frequencies only one mode is contributing to the sound propagation and can be minimized by locating error sensors at points of maximum pressure with corresponding control actuators for each uniquely phased sound wave. A more complex problem is presented when multiple modes are excited as occurs at off-resonance frequencies. Therefore, the following investigation related to broadband sound control within the duct is warranted.

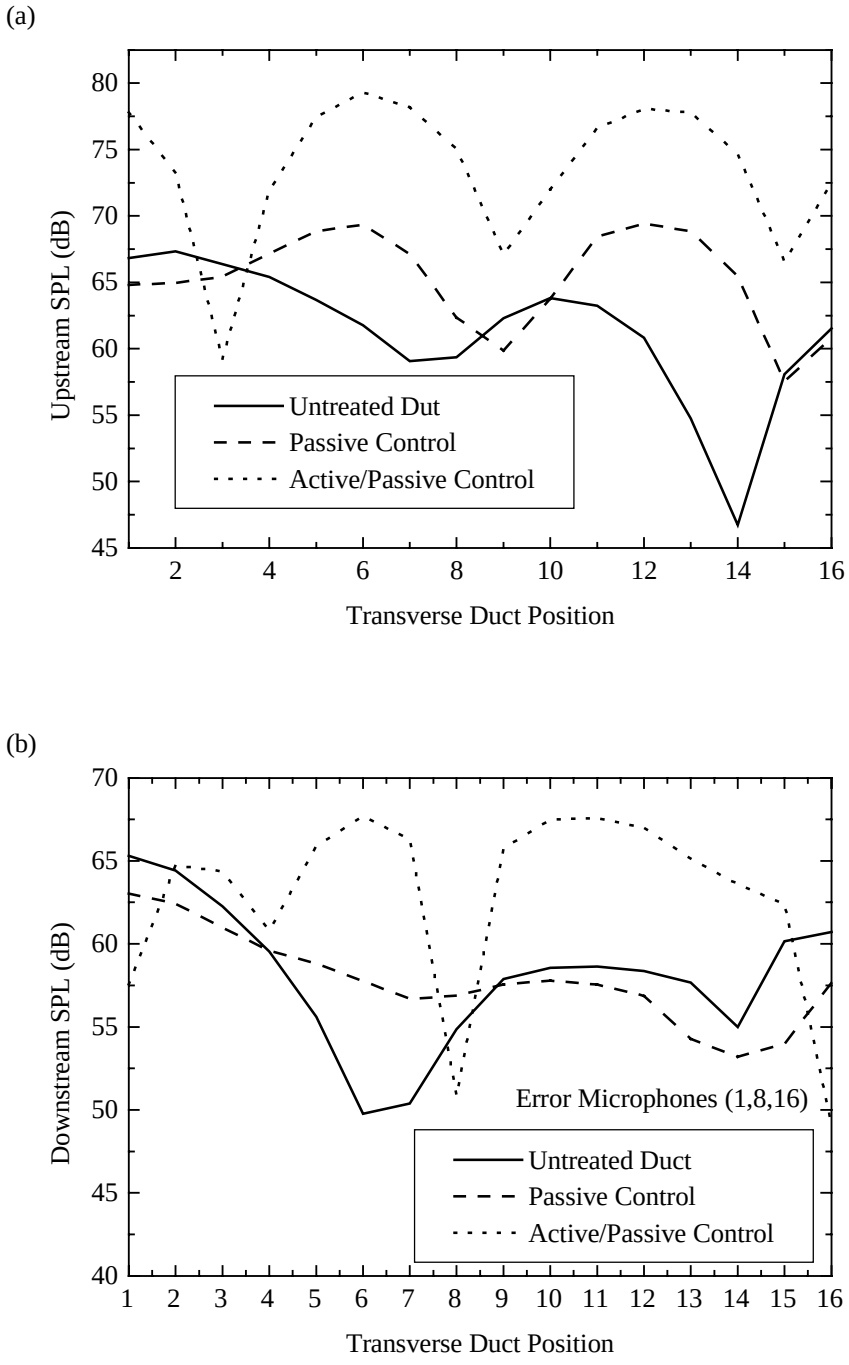

Figure 5.21: 3I3O Harmonic Control at 504 Hz with error microphones 1,8,16 (a) *Upstream* SPL vs. Transverse Duct Position. (b) *Downstream* SPL vs. Transverse Duct Position.

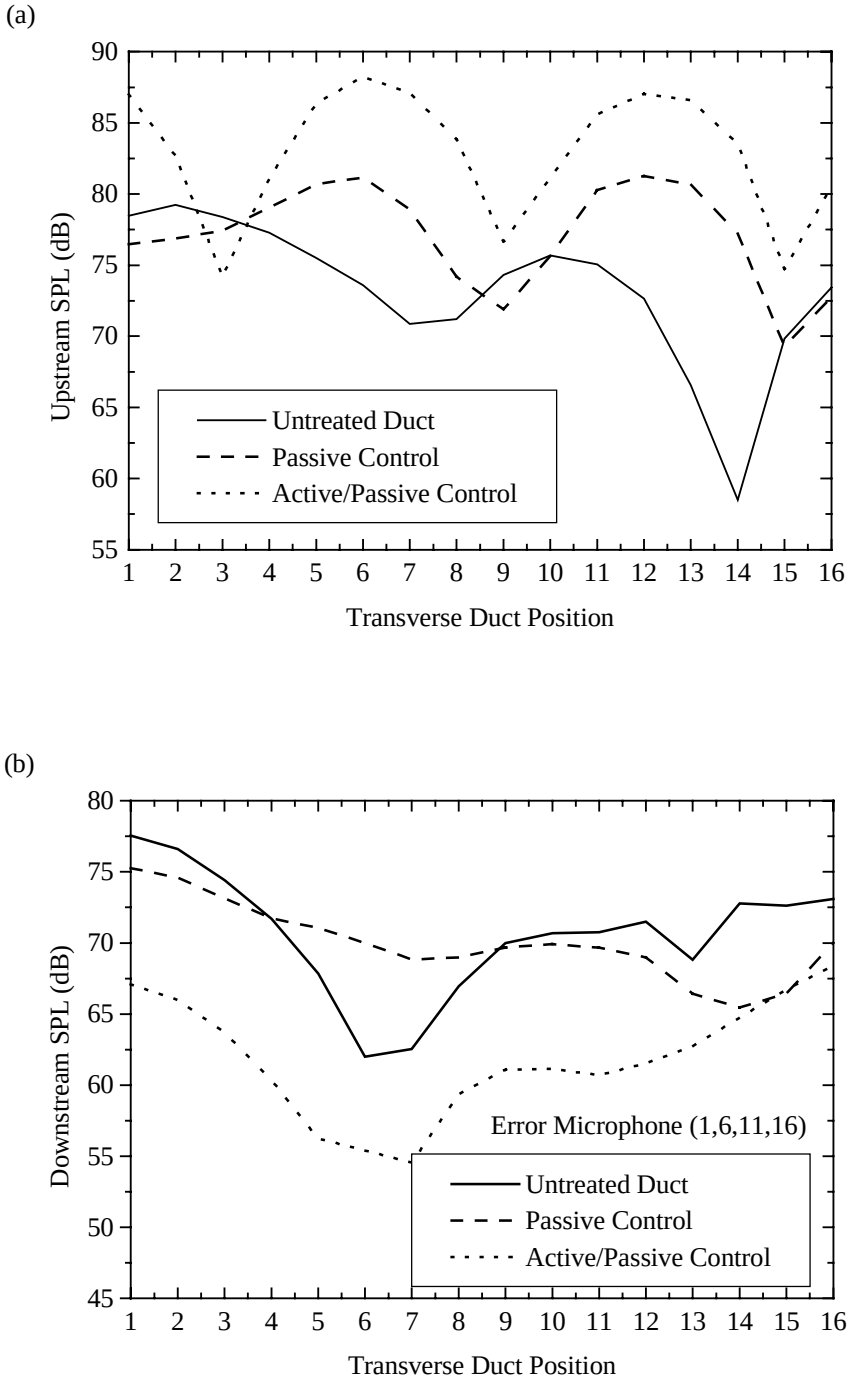

Figure 5.22: 4I3O Harmonic Control at 504 Hz with error microphones 1,6,11,16 (a) *Upstream* SPL vs. Transverse Duct Position (b) *Downstream* SPL vs. Transverse Duct Position

5.6.5 Broadband Control: 4I3O Case @ 175<f<525 Hz

In this experiment, the acoustic speaker is excited with broadband random noise between 175<f<525 Hz in order to simultaneously excite the first, second and third transverse modes of the anechoically-terminated, lined duct (see Table 5.1). The control algorithm uses a sampling frequency of 2500 Hz and 256 control filter coefficients.

The pressure is minimized at microphone's 1, 6, 11 and 16 of the downstream microphone array 4. All three smart foam actuators are employed as independent control channels. This error microphone array and smart foam distribution is chosen for two reasons. A similar configuration yielded considerable sound reduction in the harmonic control case related to the third transverse acoustic mode of the duct at 504 Hz. Secondly, using this error microphone configuration, the pressure will be minimized at uniform intervals along the transverse cross-section of the duct. This should account for global downstream sound reduction. As a measure of the smart foam control performance during broadband control, the spatially-averages mean square sound pressure is converted to dB and studied as a function of the excitation frequency. The response at *upstream* microphone arrays 1-3 are spatially averaged to monitor the upstream noise control performance yielding one value corresponding to a specific frequency. Similarly, the response at *downstream* microphone arrays 4-6 are spatially-averaged to monitor the downstream noise control performance. As in the harmonic control cases, data is recorded for the following three duct configurations: (1) Untreated Duct, (2) Passive Control, and (3) Active/Passive Control.

The global upstream sound pressure level is plotted in Figure 5.23(a) as a function of frequency using the experimental setup described previously. A passive sound reduction of approximately 5.0 dB is primarily observed near resonant frequencies of the rigid duct as the foam liner shifts the resonant frequencies of the system to lower values. The addition of active control generates some attenuation near 184 Hz which represents the first mode of the lined duct. Virtually no reduction can be attributed to the active component of smart foam upstream of the control actuators above this frequency. Some control spillover is noted, this indicates that the acoustic field generated by the downstream control actuators interact constructively with the primary source.

The global downstream sound pressure level is shown in Figure 5.23(b). Good active/passive control is observed in the 175<f<275 Hz and 350<f<450 Hz frequency ranges. These are frequency ranges where the untreated duct generates the highest sound levels. In these regions, a passive sound reduction of about 5.0 dB is noted and the active component of smart foam contributes a further 4.0 dB. Therefore, this control setup yields approximately 9.0 dB active/passive reduction downstream of the control actuators over most of the studied frequency ranges. The average rms control voltage driving each smart foam control channel is shown in Figure 5.24 as a function of frequency. In general, the control voltages are higher in the lower frequency range indicating that the smart foam has to exert more control power to minimize the sound in this frequency region. In the 250<f<350 Hz region, approximately 3.0 dB passive sound attenuation is noted, however, no active sound attenuation is noted at these frequencies. In this frequency range, the primary source generates low sound levels indicating the poor performance may be attributed to the finite digital precision of the control algorithm. Further experimental tests are warranted in this frequency range, as discussed in the following paragraph.

An additional broadband noise control test is performed to investigate obtaining improved active noise control performance in the 250<f<350 Hz bandwidth. The acoustic speaker excitation within the duct is band-limited to the 250<f<350 Hz frequency range and the same error sensor and actuator configuration is used as in the previous case. A sampling frequency of 1500 Hz with 64 control filter coefficients is implemented in the control code. The sound pressure levels associated with the global upstream microphone arrays is plotted in Figure 5.25(a). Approximately 4.0 dB passive attenuation is gained and the active smart foam input appears to exacerbate the sound levels in this upstream region of the duct. Figure 5.25(b) shows the control results downstream of the control actuators. In the studied frequency bandwidth, about 10.0 dB active/passive attenuation is gained, with about 5.0 dB attributed to passive dissipation. Comparing Figures 5.23(b) and 5.25(b) imply that global active/passive control downstream of the control actuators can be achieved in the entire 175<f<525 Hz frequency bandwidth by increasing the number of control actuators.

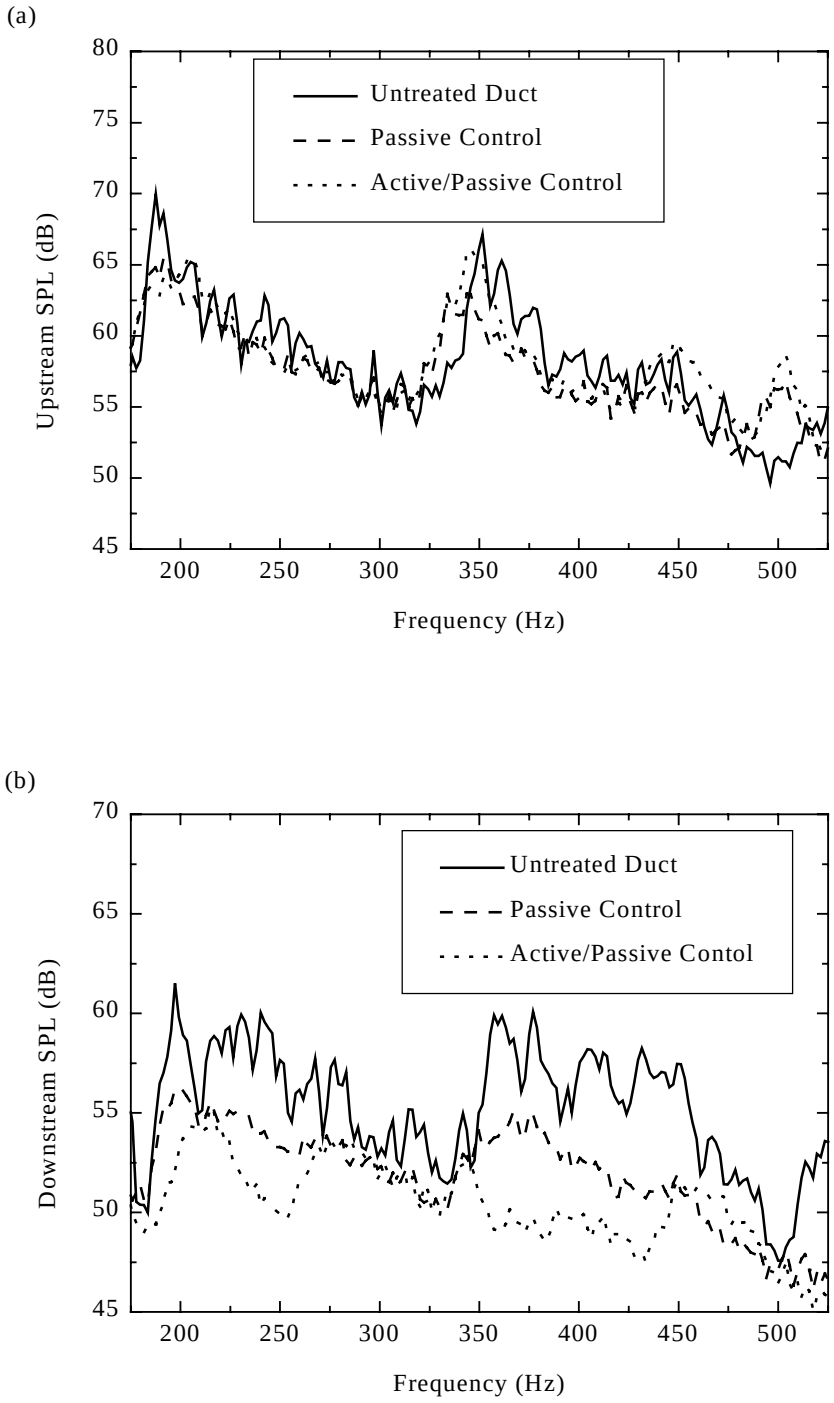

Figure 5.23: 4I3O Broadband Control 175<f<525 with error microphones 1,6,11,16 (a) *Upstream* SPL vs. Frequency (b) *Downstream* SPL vs. Frequency

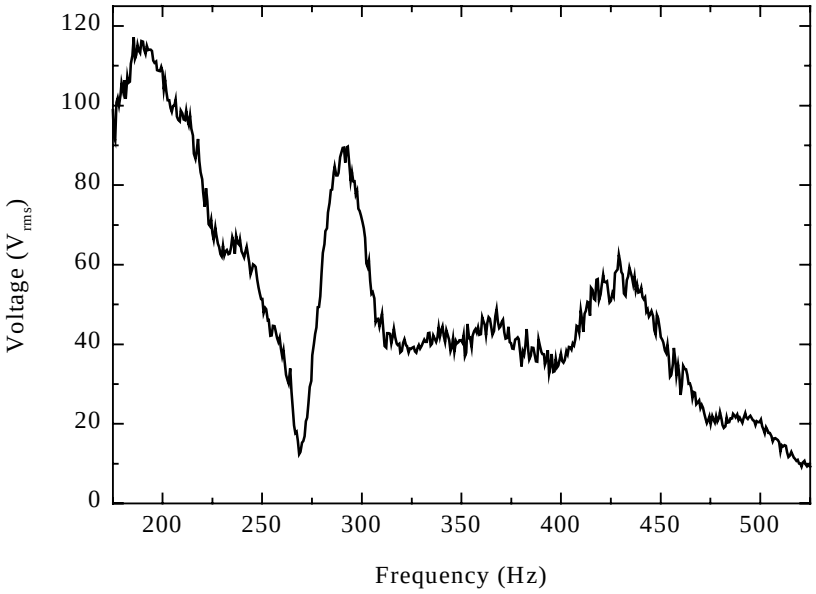

Figure 5.24: 4I3O Broadband Control at 175<f<525 with error microphones 1,6,11,16 Average Control Voltage to Smart Foam Channel 1,2 and 3 vs. Frequency.

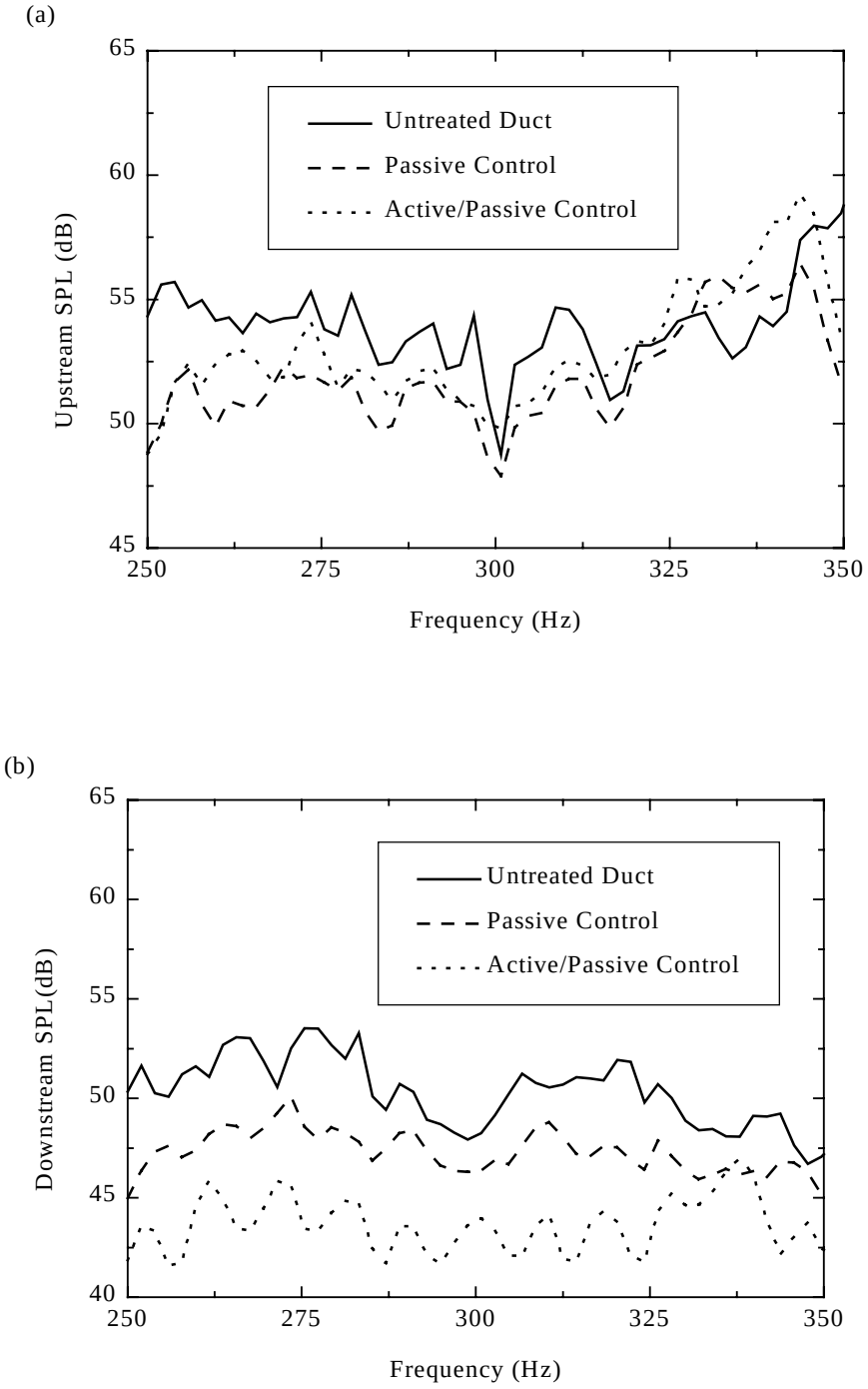

Figure 5.25: 4I3O Broadband Control 250<f<350 Hz with error microphones 1,6,11,16 (a) *Upstream* SPL vs. Frequency (b) *Downstream* SPL vs. Frequency

5.7 Comparison of Numerical and Experimental Duct Noise Control Results

The numerical results are presented to provide a very useful, quick and economical way of studying the influence of control parameters such as the quantity and orientation of error sensors and actuators. These variables can then be used to efficiently design practical noise control systems. In the following numerical duct noise control examples, the dimensions of the duct and orientation of the source, smart foam liner and error sensors are identical to those used in the experimental setup of Figure 5.11. A sample finite element mesh is illustrated in Figure 5.26. Sound pressure levels are calculated at the same axial duct locations as the six microphone arrays in the experimental study, with array 4 containing the error sensors. Six smart foam actuators are present and represent three control channels when every two neighboring actuators are wired in phase, as in the experimental study. The pressure can be minimized at three designated nodal points that are located along the cross section of the duct on array 4. As with the experimental implementation, the goal is to minimize the pressure at a discrete point or set of points along the cross section of the duct while yielding global sound attenuation in the downstream region of the duct.

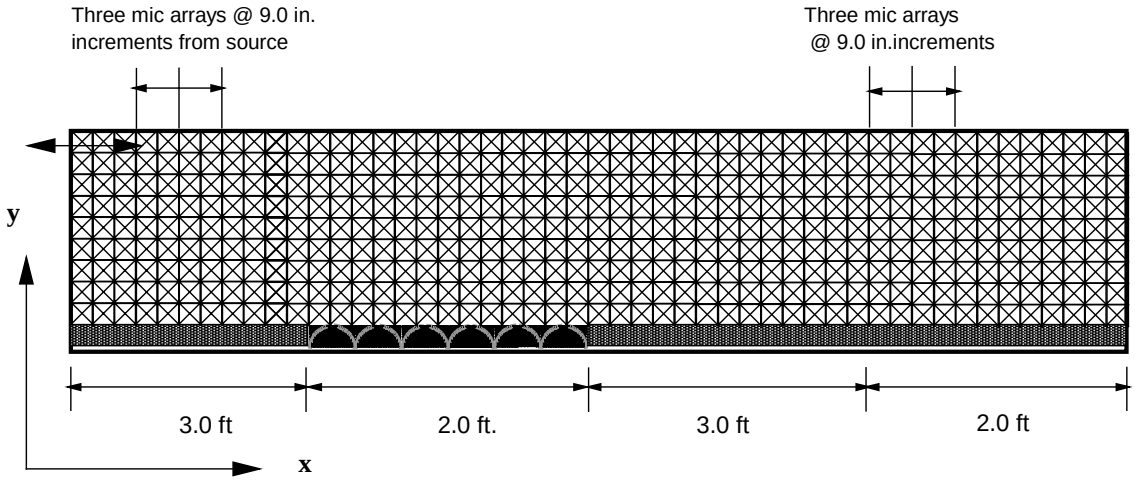

Figure 5.26: Sample finite element mesh of rectangular, anechoically-terminated duct with active/passive liner.

Optimal control theory based on transfer functions [83] is implemented to simulate a 1I1O, 2I2O, and a 3I3O control scheme to minimize the downstream sound pressure.. The test frequencies are at 188 Hz, 349 Hz, and 509 Hz which represent the

numerically determined first, second and third resonance frequency, respectively, of the anechoically-terminated, lined duct.

In each control case, the first step is to calculate the transfer function between the source and each error minimization point and between each smart foam actuator and each error minimization point. Allow H_{ej}^{p} to denote the transfer function between the jth error sensor and the source and H_{ej}^{ck} represent the transfer function between the jth error sensor and the kth smart foam control actuator. For a 1I1O control case, if the pressure at the jth error sensor during control is denoted by P_{ej}, the optimal gain for the controller, G^{ck}, is derived as

$$P_{ej} = G^{p} H_{ej}^{p} + G^{ck} H_{ej}^{ck} = 0 \tag{5.2}$$

$$G^{ck} = \frac{-\left(G^{p} H_{ej}^{p}\right)}{H_{ej}^{ck}} \tag{5.3}$$

where G^{p} is the gain related to the primary source or acoustic speaker which creates the disturbance. For a 3I3O control scheme, one needs to simultaneously minimize the pressure at all three error sensors while driving the three smart foam actuators with independent control voltages. To solve for the optimal control gains the following requirements are enforced:

$$\begin{aligned} P_{e1} &= G^{p} H_{e1}^{p} + G^{c1} H_{e1}^{c1} + G^{c2} H_{e1}^{c2} + G^{c3} H_{e1}^{c3} = 0 \\ P_{e2} &= G^{p} H_{e2}^{p} + G^{c1} H_{e2}^{c1} + G^{c2} H_{e2}^{c2} + G^{c3} H_{e2}^{c3} = 0 \\ P_{e3} &= G^{p} H_{e3}^{p} + G^{c1} H_{e3}^{c1} + G^{c2} H_{e3}^{c2} + G^{c3} H_{e3}^{c3} = 0 \end{aligned} \tag{5.4}$$

Accordingly, the necessary control gains are defined as

$$\begin{Bmatrix} G^{c1} \\ G^{c2} \\ G^{c3} \end{Bmatrix} = \frac{-G^{p}\left\{H_{e1}^{p} \;\; H_{e2}^{p} \;\; H_{e3}^{p}\right\}}{\begin{bmatrix} H_{e1}^{c1} & H_{e1}^{c2} & H_{e1}^{c3} \\ H_{e2}^{c1} & H_{e2}^{c2} & H_{e2}^{c3} \\ H_{e3}^{c1} & H_{e3}^{c2} & H_{e3}^{c3} \end{bmatrix}} \tag{5.5}$$

As in the previous experiments, the performance of smart foam in this duct noise control numerical simulation is determined by observing the global upstream and downstream sound pressure levels. The global upstream SPL is calculated by averaging the sum of the mean squared pressure in the longitudinal direction at microphone arrays

1-3 and converting to dB. A similar value related to the downstream performance is determined using the downstream microphone arrays 4-6. This procedure is repeated for three duct configurations *(1) Untreated Duct (2) Passive Control and (3) Active/Passive Control.*

The first numerical simulation is performed at 188 Hz (first transverse acoustic mode) and implements a 1I1O control scheme. The results are illustrated in Figures 5.22. For this setup, smart foam channel 1 and microphone 8 on the downstream microphone array 4 are utilized as the actuator and error sensor, respectively. Error microphone 8 is implemented because it represents the center of the duct cross section and maximum pressure level. Observing the upstream sound pressure levels in Figure 5.26(a), it is noted that passive sound reduction is primarily concentrated at the bottom wall of the duct near the passive foam liner (i.e. at regions near transverse duct position 1). The average passive reduction along the transverse cross-section of the duct is approximately 2.0 dB. This attenuation is enhanced by an additional 4.0 dB when active control is added yielding a total 6.0 dB active/passive reduction in the upstream region of the duct. The downstream sound pressure levels are illustrated in Figure 5.26(b). Approximately 2.0 dB passive sound reduction is gained as in the upstream region of the duct. Active/passive control drives the pressure to zero at the error microphone while an approximate 30.0 dB attenuation is noted at the other microphone positions.

An alternative numerical simulation at 188 Hz is performed using a 2I2O control scheme to suppress the first acoustic transverse mode of the duct.. The results are illustrated in Figures 5.27. For this setup, smart foam channel 1 and channel 2 are implemented as control actuators. Microphone 8 and microphone 16 of the downstream microphone array 4 are utilized as the error sensors. Observing the upstream sound pressure levels in Figure 5.27(a), the average passive reduction along the transverse cross-section of the duct is approximately 2.0 dB and the active component contributes a further 4.0 dB sound attenuation. Figure 5.27(b) shows the downstream control performance. During active/passive control, the sound pressure level is minimized to levels below zero dB indicating the superior performance of a 2I2O control setup relative to the previous 1I1O control scheme.

Various numerical noise control simulation are performed at 349 Hz (second transverse acoustic mode). A 1I1O control scheme is implemented and the results are illustrated in Figures 5.28. For this setup, smart foam channel 1 and microphone 8 of the downstream microphone array 4 are utilized as the actuator and error sensor, respectively. Error microphone 8 is implemented because it is near the maximum pressure of the mode shape and it is in the center of the duct. Observing the upstream sound pressure levels in Figure 5.28(a), it is noted that passive sound reduction is primarily concentrated at the bottom wall of the duct near the liner. The average passive reduction along the transverse length of the duct is approximately 2.0 dB. This attenuation is enhanced by an additional 6.0 dB when active control is added yielding a total 8.0 dB active/passive reduction in the upstream region of the duct. The downstream sound pressure level is illustrated in Figure 5.24(b). Approximately 2.0 dB passive sound reduction is gained as in the upstream case. Active/passive control drives the pressure to zero at the error microphone while an approximate 10.0 dB attenuation is noted at the other downstream microphone positions.

An alternative numerical simulation at 349 Hz is performed using a 2I2O control scheme to suppress the second transverse acoustic mode of the duct. The results are illustrated in Figures 5.29. For this setup, smart foam channel 1 and channel 2 are utilized as control actuators. Microphone 8 and microphone 16 of the downstream microphone array 4 are utilized as error sensors. These error minimization points represent maximum pressure levels relative to the mode shape at 349 Hz. Observing the upstream sound pressure levels in Figure 5.29(a), it is noted that passive sound reduction is primarily concentrated at the bottom wall of the duct near the liner. The average passive reduction along the transverse length of the duct is approximately 2.0 dB and the active component contributes a further 8.0 dB sound attenuation. Figure 5.29(b) shows the downstream performance. During active/passive control, the sound pressure level is minimized to zero dB at the error sensors. At the other dowstream microphones about a 40.0 dB sound reduction is noted.

Figures 5.30 indicates the smart foam noise control performance when a 3I3O control setup is used at 349 Hz. For this setup, all three smart foam channels are implemented and microphones 1, 8 and 16 of downstream microphone array 4 are utilized

as the actuators and error sensors, respectively. Observing the upstream sound pressure levels in Figure 5.30(a), the average passive reduction along the transverse length of the duct is approximately 2.0 dB and the active component contributes a further 8.0 dB sound attenuation.. Figure 5.30(b) indicates the downstream control performance and indicates that most of the passive control occurs in a localized are near the bottom wall of the duct.. During active/passive control, the sound pressure level is minimized below zero dB, indicating the superior performance of a 3I3O control setup to minimize the third transverse acoustic mode of the duct.

Several numerical simulation are performed to investigate the smart foam noise control performance at 509 Hz (third transverse mode of the duct) within the duct. Figures 5.31 illustrate the performance of a 1I1O control setup implementing smart foam control channel 1 and microphone 8 of downstream array 4 as the error sensor. As shown in Figure 5.31(a), an average 4.0 dB passive sound attenuation is observed along the transverse cross section of the duct in the upstream region. Again, the region near the bottom wall of the lined duct exhibits the highest passive attenuation. Approximately, 7.0 dB active/passive attenuation is noted in this upstream region. Figure 5.31(b) illustrates the downstream control performance for the 1I1O control case. Again, about 4.0 dB passive attenuation is achieved as in the upstream case. The sound pressure level is reduced to zero dB at the error sensor and 3.0 dB sound attenuation is gained at the other microphone positions.

Figures 5.32 illustrate the active/passive control results achieved using a 2I2O control scheme. Smart foam control channel 1 and channel 2 are implemented as control actuators. Microphone 8 and microphone 16 of downstream microphone array 4 are implemented. The results related to the upstream region of the duct are shown in Figure 5.32(a). As seen at the other test frequencies, the greatest passive sound attenuation is concentrated near the bottom wall of the lined duct. An average passive attenuation of 4.0 dB is gained along the transverse cross-section of the duct. The addition of active control causes some control spillover resulting in a 3.0 dB increase in sound levels. The downstream control results are shown in Figure 5.32(b) and reveal similar passive control results. However, the addition of active control reduces the sound levels at each

error sensor to zero dB while little or no active control is observed at the other microphone positions.

A 3I3O control scheme is investigated to minimize the pressure within the duct at 509 Hz. The control setup utilizes all three smart foam channels and incorporates microphone 1, 8 and 16 on downstream array 4 as the error sensors. The upstream control results are plotted in Figure 5.33(a). As expected, about a 4.0 dB passive attenuation is gained as observed in the other control cases at 509 Hz. The addition of active control generates a further 3.0 dB sound reduction. Figure 5.33(b) indicates the downstream control performance. Similar passive control reduction is gained when compared to the upstream control results. Active/passive control reduces the sound pressure levels at the error sensors to below zero dB. At the other erro microphone positions about a 60 dB sound attenuation is noted. Consequently, the active/passive 3I3O control scheme at 509 Hz virtually reduces the downstream sound levels along the transverse section of the duct to zero dB compared to the other control setups.

It is necessary to compare the smart foam control performance and trends observed in the numerical simulations to the experimental duct acoustic control results. The comparison is based on the efficient suppression of the transverse propagating modes within the anechoically-terminated duct. The numerical and experimental duct acoustic control results illustrate that the addition of the passive foam liner to the bottom duct wall alters the mode shape compared to the mode shape of the untreated duct. This is most prevalent in the higher frequency region and is attributed to the soft impedance of the foam liner compared to the rigid duct wall. The addition of the passive liner can reduce the global sound levels within the duct and reduction appears to be a maximum near the lined bottom duct wall. Passive sound attenuation increases as the ratio of the acoustic wavelength to passive liner length decreases. This indicates that an acoustic propagating wave will experience a significant loss of acoustic energy in the high-frequency range which is the intent of smart foam. It is discovered that the best control results are achieved when the dimension of the control system (i.e. the number of error sensors and control channels) is equal to the order of the mode one is trying to control. For significant reduction, the error sensors are located at points of maximum sound

pressure levels. In all studies it is evident that significant downstream sound reduction within the duct may be achieved at the expense of increasing the upstream sound levels during active control.

.

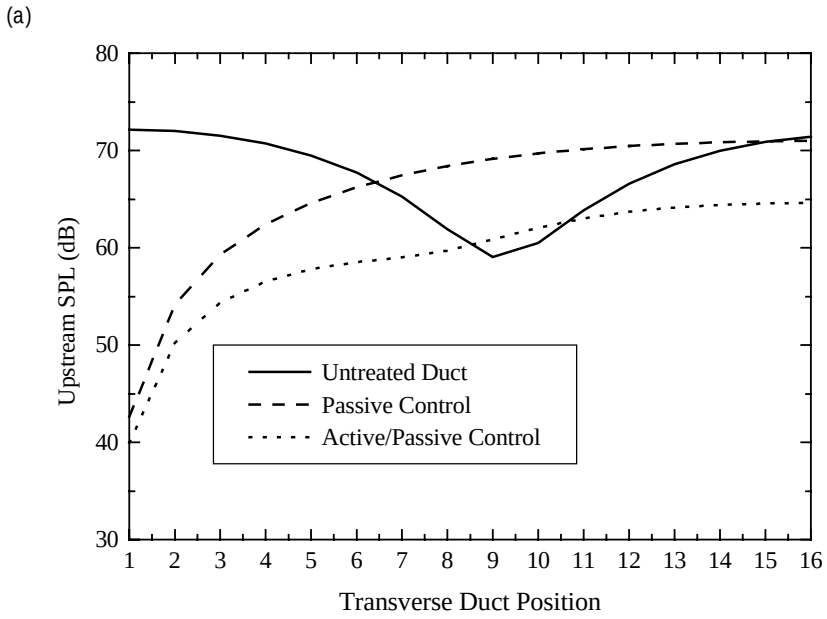

.

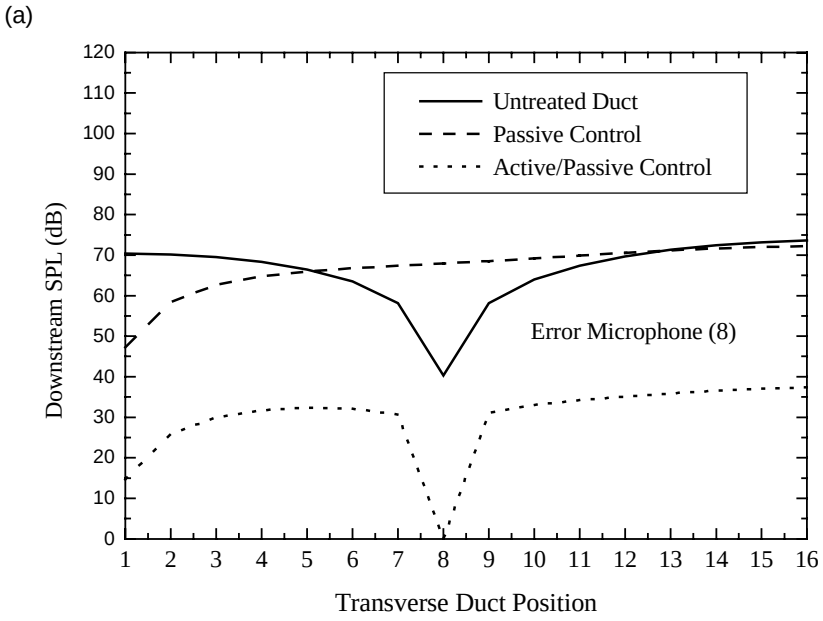

Figure 5.26: 1I1O Harmonic Control @ 188 Hz (a) Upstream SPL vs. Transverse Duct Position (b) Downstream SPL vs. Transverse Duct Position.

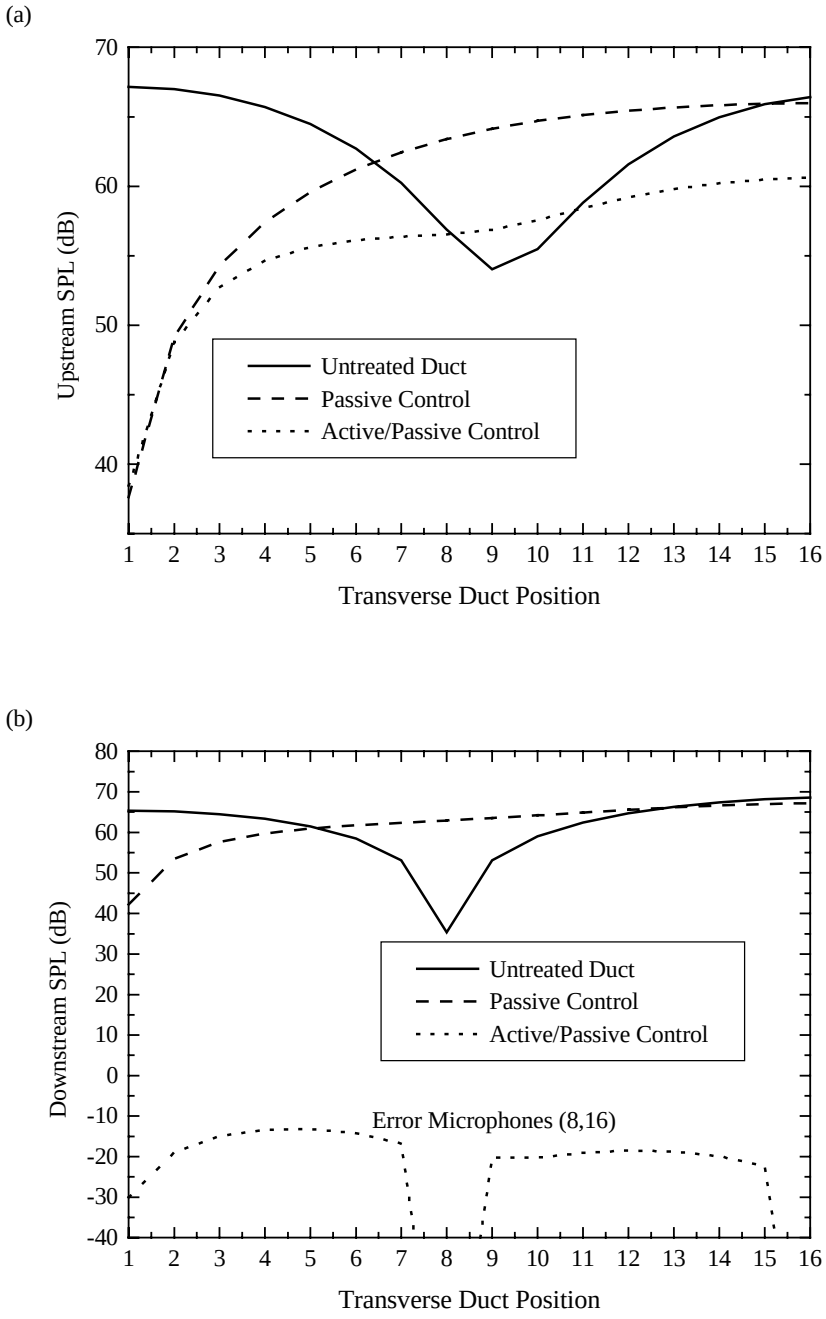

Figure 5.27: 2I2O Harmonic Control @ 188 Hz (a) Upstream SPL vs. Transverse Duct Position (b) Downstream SPL vs. Transverse Duct Position.

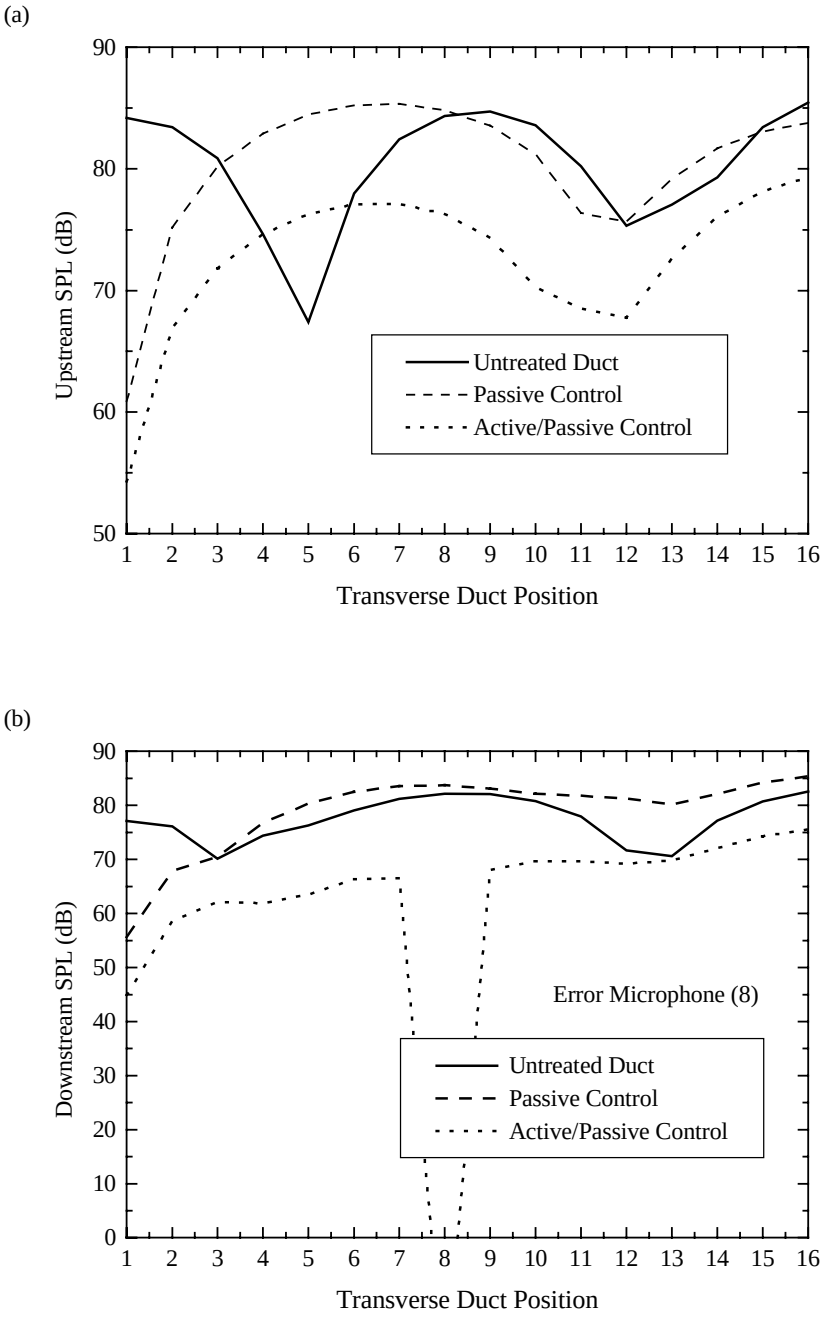

Figure 5.28: 1I1O Harmonic Control @ 349 Hz (a) Upstream SPL vs. Transverse Duct Position (b) Downstream SPL vs. Transverse Duct Position.

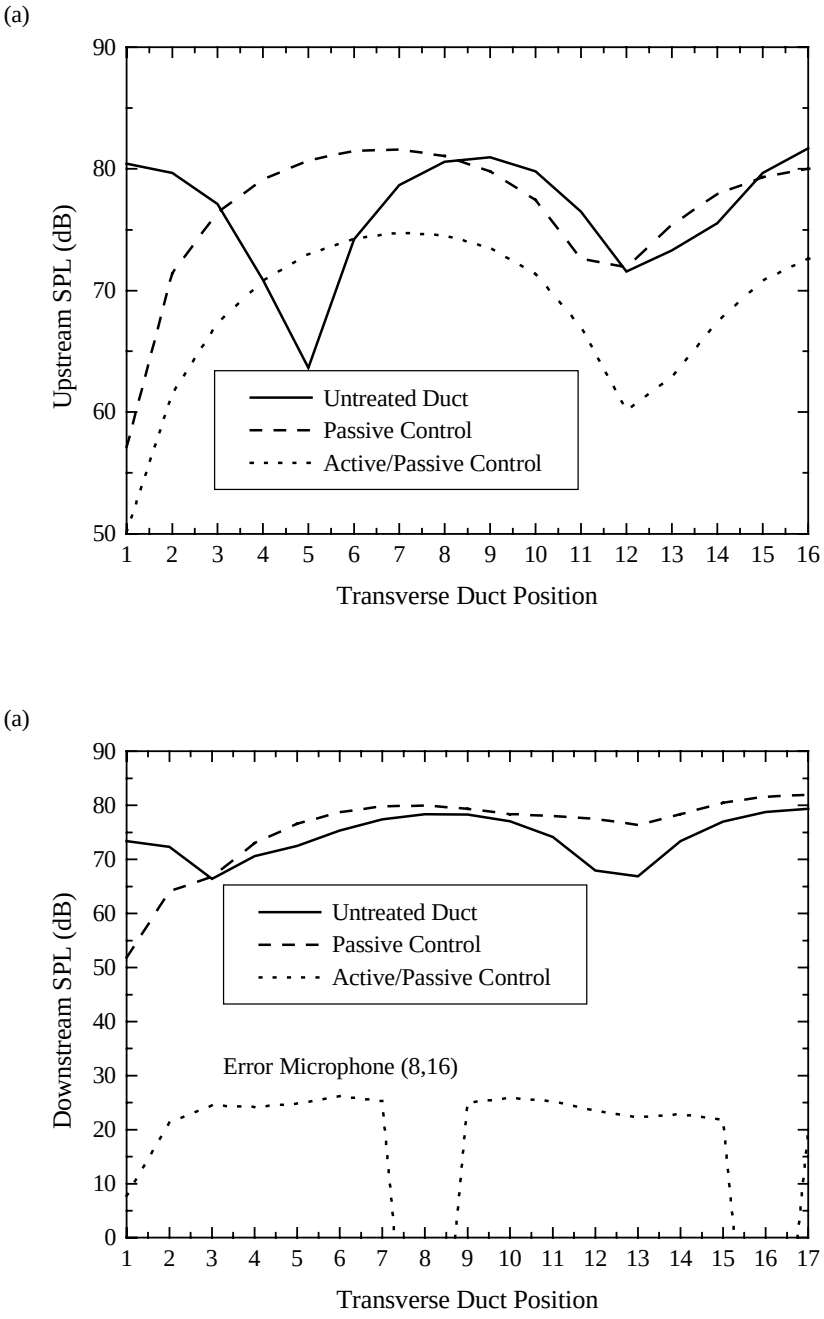

Figure 5.29: 2I2O Harmonic Control @ 349 Hz (a) Upstream SPL vs. Transverse Duct Position (b) Downstream SPL vs. Transverse Duct Position.

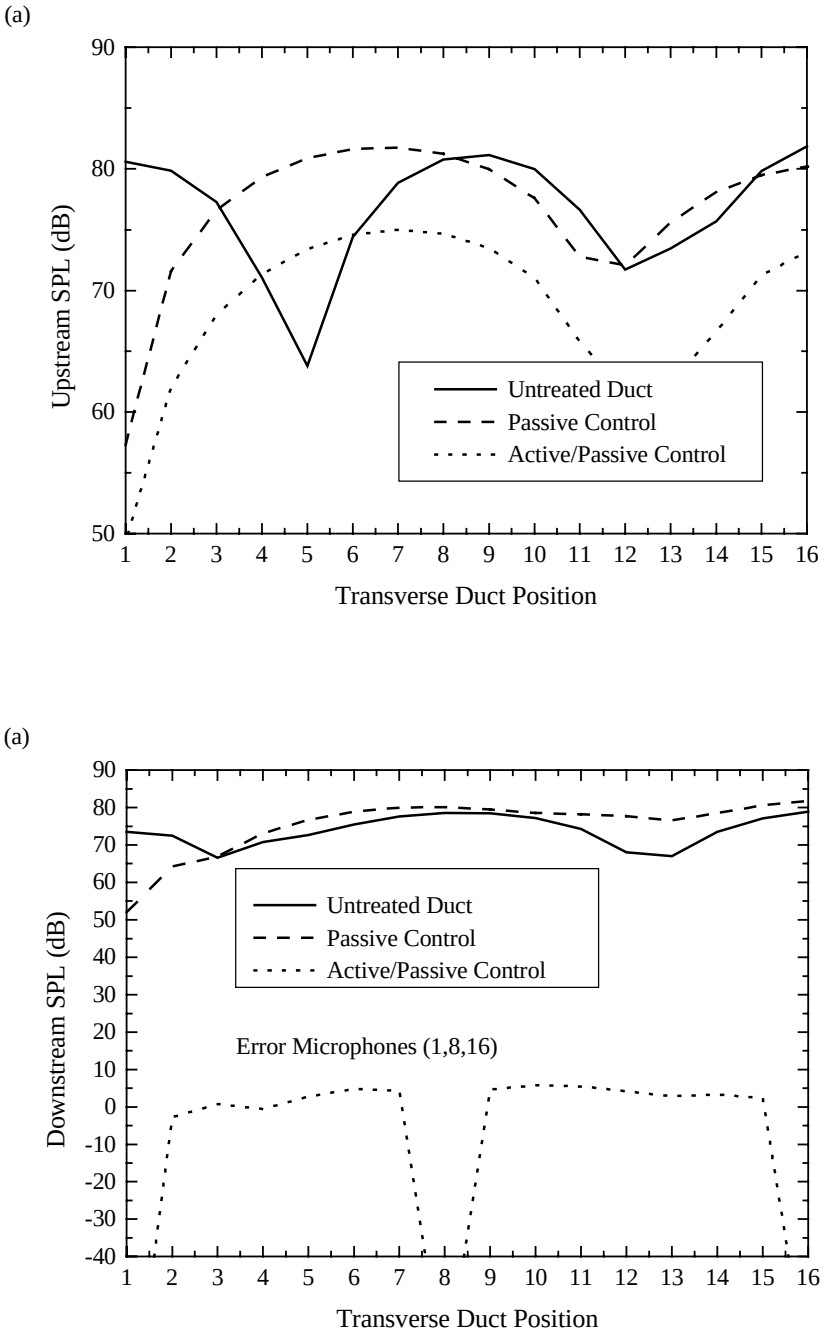

Figure 5.30: 3I3O Harmonic Control @ 349 Hz (a) Upstream SPL vs. Transverse Duct Position (b) Downstream SPL vs. Transverse Duct Position.

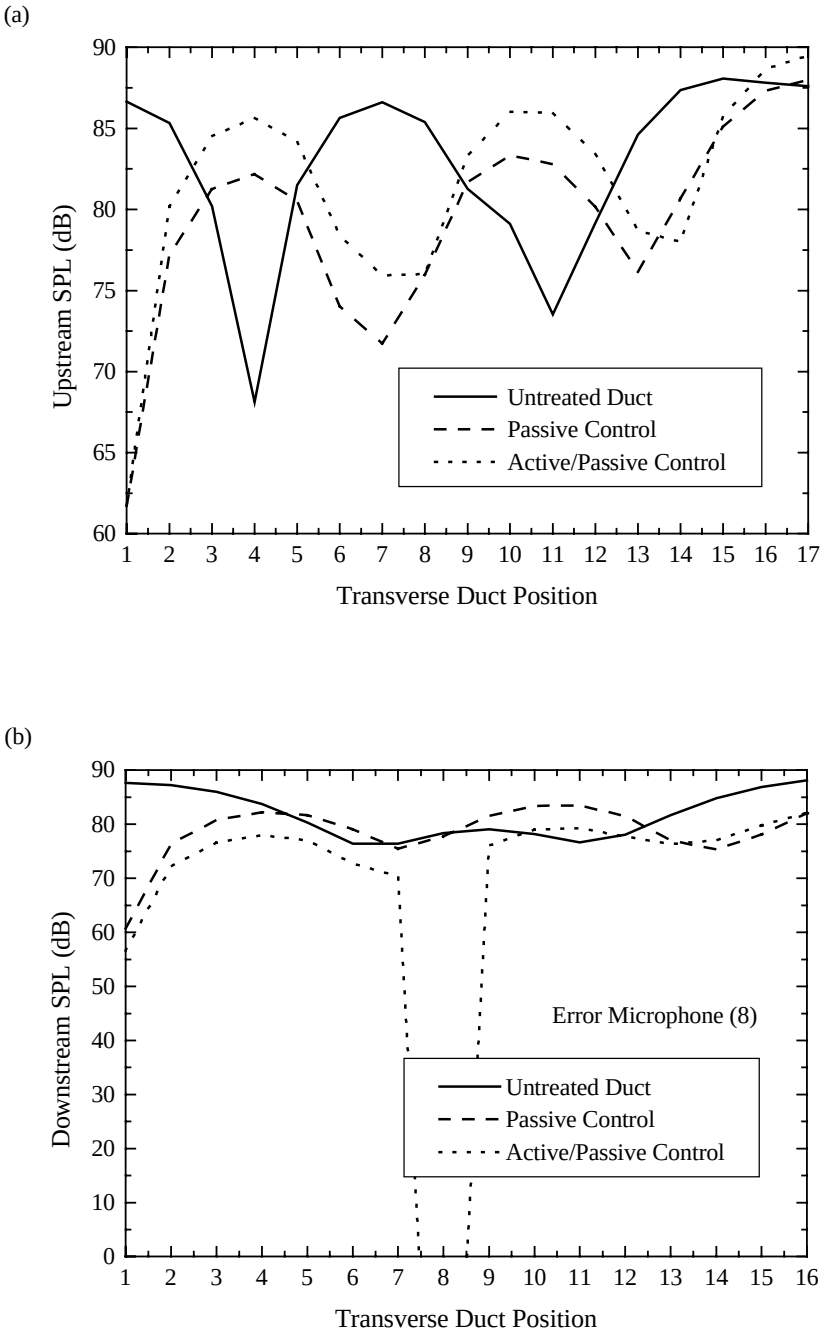

Figure 5.31: 1I1O Harmonic Control @ 509 Hz (a) Upstream SPL vs. Transverse Duct Position (b) Downstream SPL vs. Transverse Duct Position.

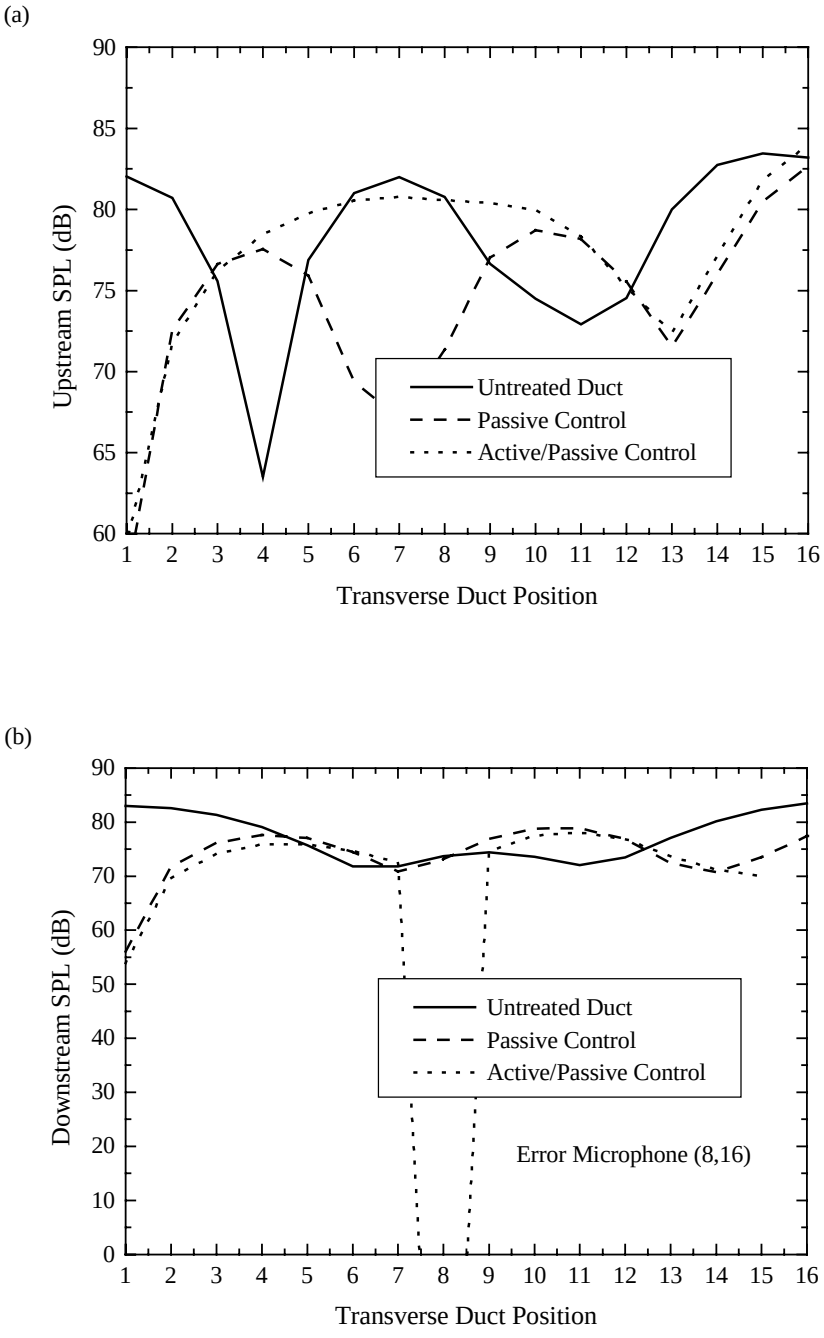

Figure 5.32: 2I2O Harmonic Control @ 509 Hz (a) Upstream SPL vs. Transverse Duct Position (b) Downstream SPL vs. Transverse Duct Position.

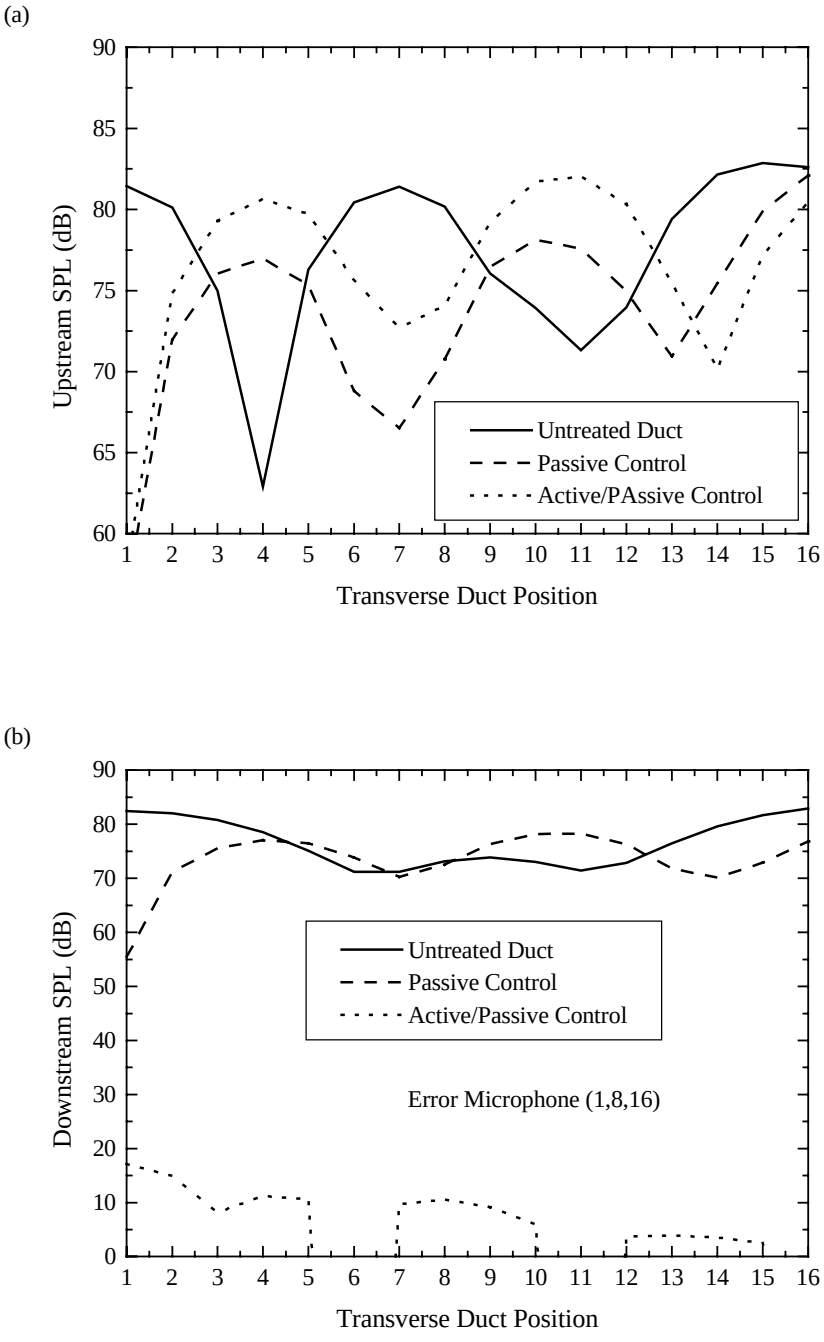

Figure 5.33: 3I3O Harmonic Control @ 509 Hz (a) Upstream SPL vs. Transverse Duct Position (b) Downstream SPL vs. Transverse Duct Position.

5.8 ***Summary***

This chapter presented experimental results implementing a smart foam liner to suppress the propagating waves in a rigid duct with an anechoic termination. A preliminary modal analysis revealed that the effects of the passive liner are predominately observed at the system resonance's in the higher frequency range. At these frequencies, a substantial decrease in sound pressure is noted due to damping effects. Furthermore, the resonant frequencies of a passively lined duct are lower than those of the untreated duct. This observation is due to a decrease in stiffness of the system once the duct wall is lined with foam. Several control schemes based on the Filtered-x, feedforward control algorithm are implemented to suppress propagating waves associated with the first, second and third transverse resonance frequencies of the system. These control schemes range form a 2I2O control setup to a 4I3O control setup. In general, it was found that in order to achieve substantial global sound attenuation, the number of error sensors and actuators should equal the order of the mode one wishes to control. Specifically, the order of the mode corresponds to the number of uniquely-phased sound waves propagating within the duct to formulate a particular mode. Several numerical noise control simulations are presented in this chapter. As in the experimental study, it is revealed that the passive liner can contribute global sound reduction downstream of the control actuators. Significant passive sound attenuation is noted near the bottom wall of the lined duct. Good active sound control is gained when the dimensions of the controller are equal to the transverse modal order. Furthermore, to ensure global downstream sound attenuation, error sensors should be located within regions of maximum sound levels along the transverse cross sections of the duct.